AD-A032 365 NAVAL POSTGRADUATE SCHOOL MONTEREY CALIF F/G 11/6
MICROSCOPIC INVESTIGATION OF INTERFACE CORROSION OF STEEL-ALUMI--ETC(U)
SEP 76 M R KEELEAN

UNCLASSIFIED NL

1 OF 2

AD
A032365

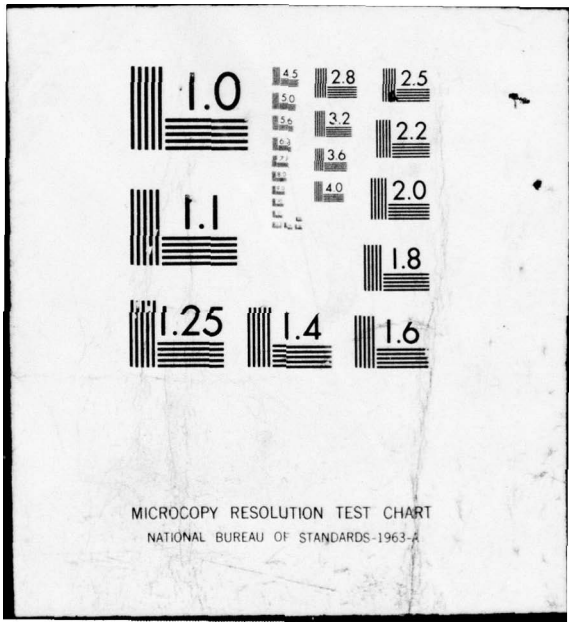
1.0
1.1
1.25
1.4
1.6
1.8
2.0
2.2
2.5
2.8
3.2
3.6
4.0
4.5
5.0
5.6
MICROCOPY RESOLUTION TEST CHART
NATIONAL BUREAU OF STANDARDS-1963-A

NAVAL POSTGRADUATE SCHOOL
Monterey, California

THESIS

MICROSCOPIC INVESTIGATION OF INTERFACE CORROSION OF STEEL-ALUMINUM EXPLOSIVELY BONDED MATERIAL EXPOSED TO PERIODIC SEA WATER SPRAY

by

Michael Richard Keelean

September 1976

Thesis Advisor: A. J. Perkins

SECURITY CLASSIFICATION OF THIS PAGE (When Date Entered)

REPORT DOCUMENTATION PAGE

READ INSTRUCTIONS BEFORE COMPLETING FORM

1. REPORT NUMBER	2. GOVT ACCESSION NO.
3. RECIPIENT'S CATALOG NUMBER	
4. TITLE (and Subtitle) (6) Microscopic Investigation of Interface Corrosion of Steel-Aluminum Explosively Bonded Material Exposed to Periodic Sea Water Spray.	5. TYPE OF REPORT & PERIOD COVERED (9) Master's Thesis; September 1976
	6. PERFORMING ORG. REPORT NUMBER
7. AUTHOR(s) (10) Michael Richard Keelean	8. CONTRACT OR GRANT NUMBER(s)
9. PERFORMING ORGANIZATION NAME AND ADDRESS Naval Postgraduate School Monterey, California 93940	10. PROGRAM ELEMENT, PROJECT, TASK AREA & WORK UNIT NUMBERS (12) 132 p.
11. CONTROLLING OFFICE NAME AND ADDRESS Naval Postgraduate School Monterey, California 93940	12. REPORT DATE (11) September 1976 13. NUMBER OF PAGES 132
14. MONITORING AGENCY NAME & ADDRESS(if different from Controlling Office) Naval Postgraduate School Monterey, California 93940	15. SECURITY CLASS. (of this report) Unclassified 15a. DECLASSIFICATION/DOWNGRADING SCHEDULE

16. DISTRIBUTION STATEMENT (of this Report)

Approved for public release; distribution unlimited.

17. DISTRIBUTION STATEMENT (of the abstract entered in Block 20, if different from Report)

18. SUPPLEMENTARY NOTES

19. KEY WORDS (Continue on reverse side if necessary and identify by block number)

20. ABSTRACT (Continue on reverse side if necessary and identify by block number)

An explosively bonded triclad consisting of 5456 aluminum, 1100 aluminum, and ASTM A516, Grade 55 steel is currently in use as a transition joint between steel hulls and aluminum superstructures on several military marine vehicles. This study examines some of the corrosion processes and product formations that take place when this joint is exposed to the marine atmosphere. Accelerated sea spray testing was performed

DD FORM 1 JAN 73 1473 (Page 1) EDITION OF 1 NOV 65 IS OBSOLETE S/N 0102-014-6601

SECURITY CLASSIFICATION OF THIS PAGE (When Date Entered)

251 450

in the laboratory to simulate in-service conditions with joint specimens receiving exposures of varying durations. A corrosion model is hypothesized and photomicrographs of the various exposed specimens are presented and discussed.

Microscopic Investigation of Interface Corrosion of Steel-Aluminum Explosively Bonded Material Exposed to Periodic Sea Water Spray

by

Michael Richard Keelean
Lieutenant, United States Navy
B.S., Central Michigan University, 1968

Submitted in partial fulfillment of the requirements for the degree of

MASTER OF SCIENCE IN MECHANICAL ENGINEERING

from the

NAVAL POSTGRADUATE SCHOOL
September 1976

Author Michael R. Keelean

Approved by: Jeff Perkins
Thesis Advisor

Terry R. McNelley
Second Reader

Allen E. Fuhs
Chairman, Department of Mechanical Engineering

J. R. Borsting
Academic Dean

ABSTRACT

An explosively bonded triclad consisting of 5456 aluminum, 1100 aluminum, and ASTM A516, Grade 55 steel is currently in use as a transition joint between steel hulls and aluminum superstructures on several military marine vehicles. This study examines some of the corrosion processes and product formations that take place when this joint is exposed to the marine atmosphere. Accelerated sea spray testing was performed in the laboratory to simulate in-service conditions with joint specimens receiving exposures of varying durations. A corrosion model is hypothesized and photomicrographs of the various exposed specimens are presented and discussed.

TABLE OF CONTENTS

I. INTRODUCTION - 16

A. THE EXPLOSIVE BONDING PROCESS - - - - - - - - 16

B. USES OF EXPLOSIVELY BONDED MATERIALS - - - - 21

C. PREVIOUS TESTING - - - - - - - - - - - - - - - 27

D. ELECTROCHEMICAL BACKGROUND - - - - - - - - - - 29

E. CORROSION MODEL - - - - - - - - - - - - - - - - 42

II. EXPERIMENTAL STRUCTURE - - - - - - - - - - - - - - 47

A. APPARATUS - - - - - - - - - - - - - - - - - - - 47

1. Tank Assembly - - - - - - - - - - - - - - - 47

2. Microscopes - - - - - - - - - - - - - - - - 52

B. PROCEDURES - - - - - - - - - - - - - - - - - - - 55

III. RESULTS AND DISCUSSION - - - - - - - - - - - - - - 58

A. UNEXPOSED SAMPLES - - - - - - - - - - - - - - - 58

B. SHORT TERM EXPOSURE - - - - - - - - - - - - - - 66

C. LONG TERM EXPOSURE - - - - - - - - - - - - - - - 114

IV. CONCLUSIONS - 127

V. RECOMMENDATIONS - - - - - - - - - - - - - - - - - - 129

LIST OF REFERENCES - - - - - - - - - - - - - - - - - - - 130

INITIAL DISTRIBUTION LIST - - - - - - - - - - - - - - - 132

LIST OF TABLES

Table 1. Standard oxidation-reduction potentials - - - 30

Table 2. Galvanic series of some commercial metals and alloys in seawater - - - - - - - - - 34

LIST OF FIGURES

Figure 1. Illustration of rippling phenomenon during explosive bonding - - - - - - - - - - - 19

Figure 2. Explosive-metal geometries utilized to accomplish explosive bonding - - - - - - - 20

Figure 3. Mechanical fastening technique - - - - - - - - 24

Figure 4. Typical explosively bonded joint with webs - - - - - - - - - - - - - - - - - - - 25

Figure 5. Typical aluminum superstructure and steel deck connection demonstrating the use of welding transition joints - - - - 26

Figure 6. Kinetics of the growth of oxide films on various metals at room temperature in oxygen or dry air - - - - - - - - - - - - - 33

Figure 7. Dependence of atmospheric corrosion on thickness of the moisture film on the metal surface - - - - - - - - - - - - - - 37

Figure 8. Anodic polarization curve for a specimen exhibiting passivity, determined potentiostatically - - - - - - - - 39

Figure 9. The effect of chloride ion upon the anodic polarization curve for a metal that exhibits passivity - - - - - - - - - - - 41

Figure 10. Corrosion model - - - - - - - - - - - - - - - - 43

Figure 11. Pourbaix diagram shows theoretical conditions for corrosion of metallic iron - - - - - - - - - - - - - - - - - 44

Figure 12. Pourbaix diagram shows theoretical conditions for corrosion of aluminum - 44

Figure 13. Tank with one rim assembly removed and placed on top - - - - - - - - - - - - - - 49

Figure 14. Close-up of rim assembly and installed sample - - - - - - - - - - - - - - - - 50

Figure 15. Rim assembly and nozzle installed in chamber - - - - - - - - - - - - 51

Figure 16. Cambridge Model S4-10 Scanning Electron Microscope (SEM) and attached Princeton Gamma-Tech PGT-1000 X-ray Analyzer - - - - - - - - - - - 53

Figure 17. 5.5x binocular photomicrograph of a polished 12.5 mm-square segment of standard test sample (5456 Al-top, 1100 Al-middle, ASTM A516 Steel-bottom) - - - - - - - - - - - - - - - - - 59

Figure 18. 7x binocular photomicrograph of steel-aluminum bond (Aluminum-top, steel-bottom). Sample held in bakelite mount - - - - - - - - - - - - - - - 61

Figure 19. 20x binocular photomicrograph of steel wave with melt (Aluminum over Steel) - - - - - - - - - - - - - - - - - 63

Figure 20. 50x B&L Bench Metallograph photo of steel wave and melt. Dark porous material around the top is aluminum. White material is steel. Gray material is melt - - - - - - - - - - - - - - - 64

Figure 21. 320x SEM photograph of steel-aluminum interface in the as-sanded condition (Steel←→Al) - - - - - - - - - - - - - - - - - 65

Figure 22. 320x SEM photograph of unexposed aluminum half of typical sample in an as-sanded condition - - - - - - - - - - 67

Figure 23. 320x SEM photograph of unexposed steel of a typical sample in an as-sanded condition - - - - - - - - - - - - 68

Figure 24. 160x SEM picture of the interface region showing corrosion band after 30-minute exposure and six sprayings (Steel←→Al) - - - - - - - - - - - - - - - - - 69

Figure 25. 170x SEM picture of the interface region showing corrosion band after 30-minute exposure and 15 sprayings (Steel←→Al) - - - - - - - - - - - - - - - - - 70

Figure 26. 250x SEM picture of bond area and corrosion belt showing localized anodic dissolution after 30-minute exposure and 15 sprayings (Steel←→Al) - - 72

Figure 27. 320x SEM photograph of aluminum away from interface after 30-minute exposure and 15 sprayings - - - - - - - - - 73

Figure 28. 320x SEM photograph of aluminum away from interface after 30-minute exposure and six sprayings - - - - - - - - 74

Figure 29. 340x SEM picture of steel away from bond after 30-minute exposure and six sprayings - - - - - - - - - - - - - - - - - 75

Figure 30. 320x SEM picture of steel away from bond showing initiation of rust deposits after 30-minute exposure and 15 sprayings - - - - - - - - - - - - - - 76

Figure 31. 175x SEM photograph of the interface illustrating the corrosion band and small clumps of rust after one-hour exposure and 30 sprayings (Steel←→Al) - - 78

Figure 32. 25x SEM photograph showing the bond interface with trail of white deposits on the steel after one-hour exposure and 12 sprayings (Steel←→Al) - - 79

Figure 33. 250x SEM picture of interface showing small deposits on steel after one-hour exposure and 12 sprayings (Steel←→Al) - - 80

Figure 34. 1100x SEM photograph of interface showing snowflake-like build-up on steel with no build-up on aluminum. Sample had one-hour exposure and 12 sprayings (Steel←→Al) - - - - - - - - - - 81

Figure 35. 1300x SEM picture of interface after one-hour exposure and 12 sprayings shows microanodic valley - - - - - - - - - 82

Figure 36. 260x SEM photograph of aluminum taken after one-hour exposure and 12 sprayings. It shows slightly hazed tone of fringes - - - - - - - - - - - - - - - - - 84

Figure 37. 320x SEM picture of aluminum taken after a one-hour exposure and 30 sprayings. Shows hazy tone of fringes - - - - - - - - - - - - - - - - - - - 85

Figure 38. 290x SEM photograph of interface after two-hour exposure showing belt zone and adjacent films (Steel←→Al) - - - 87

Figure 39. 300x SEM picture of interface after two-hour exposure showing hazy film coverage over most areas (Steel←→Al) - - 88

Figure 40. 300x SEM photograph of aluminum after two-hour exposure. It shows general surface deterioration and loss of features - - - - - - - - - - - - - - - - - - 90

Figure 41. 75x SEM picture of rust nodules formed over layer of alumina film on steel after two-hour exposure - - - - - - - - - - 91

Figure 42. 700x SEM picture of beginning of rusting at surface deformity on steel after two-hour exposure - - - - - - - - - - - - - - 92

Figure 43. 1050x SEM picture of rust particles on steel surface after two-hour exposure - - - 93

Figure 44. 305x SEM picture of bond area after six-hour exposure shows heavy corrosion obscuring the interface (Steel←→Al) - - - 95

Figure 45. 1350x SEM photograph of bond area after six-hour exposure showing general scale growth on the steel and a base scale growth starting to cover the aluminum (Steel←→Al) - - - - - - - - - - - - - - - - - 96

Figure 46. 250x SEM picture of the surface film over aluminum after six-hour exposure - - - 97

Figure 47. 2800x SEM picture of alumina scale on aluminum after six-hour exposure - - - - - 98

Figure 48. 2700x SEM picture of alumina precipitated onto the steel after six-hour exposure - - - - - - - - - - - - - - - - - - 99

Figure 49. 280x SEM picture of the bond interface area after 12-hour exposure (Steel←→Al) - 101

Figure 50. 1200x SEM picture of bond area after 12-hour exposure (Steel←→Al) - - - - - - - 102

Figure 51. 240x SEM picture of aluminum after 12-hour exposure - - - - - - - - - - - - - - 103

Figure 52. 2400x SEM picture of aluminum surface film after 12-hour exposure - - - - - - - - 104

Figure 53. 130x SEM picture of steel with coating of alumina and rust nodules after 12-hour exposure - - - - - - - - - - - - - - 105

Figure 54. 280x SEM picture showing iron oxide growth in alumina coating on steel after 12-hour exposure - - - - - - - - - - - - - - - - - - 106

Figure 55. 2050x SEM picture showing iron oxide growth through film of alumina on steel after 12-hour exposure - - - - - - - 107

Figure 56. 600x SEM photograph of rust and alumina formation on steel after 12-hour exposure - - - - - - - - - - - - - - - - - - 108

Figure 57. 320x SEM picture of bond interface area after one-day exposure (Steel←→Al) - - - - - - - - - - - - - - - - - 109

Figure 58. 1600x SEM picture of bond area showing complete coverage by alumina after one-day exposure (Steel←→Al) - - - - - - 110

Figure 59. 160x SEM picture of alumina on aluminum surface after one-day exposure - - - - - - 111

Figure 60. 65x SEM picture of rusting on steel half of sample after two-day exposure - - - 112

Figure 61. 1300x SEM picture of rust exploding through layer of alumina scale after two-day exposure - - - - - - - - - - - - - 113

Figure 62. 28x SEM picture of bond zone on five-week exposure specimen showing scaly corrosion product and void (Al over Steel) - - - - - - - - - - - - - - - 115

Figure 63. 280x SEM picture of alumina layer beneath second corrosion product film on five-week exposure sample. (Steel surface) - - - - - - - - - - - - - - - 117

Figure 64. 28x SEM photograph of bond zone on five-week exposure sample showing void and wave outline (Al over Steel) - - - 118

Figure 65. 28x SEM picture of bond zone on five-week exposure sample with void, wave outline, and mushroom-shaped formation (Al over Steel) - - - - - - - - - 119

Figure 66. 280x SEM picture of bond zone passivation at trailing edge of wave of five-week exposure sample (Al over Steel) - 121

Figure 67. 27x SEM photograph of mushroom-shaped corrosion product on five-week exposure sample - 122

Figure 68. 27x SEM picture of nine-week exposure sample showing pitting and mushroom corrosion product build-up (Al over Steel)- 123

Figure 69. 27x SEM picture of nine-week exposure sample showing mushroom corrosion growth and melt pitting in wave (Al over Steel) - 124

Figure 70. 27x SEM picture of nine-week exposure sample showing pitting, corrosion product growth, and wave outline (Al over Steel) - - - - - - - - - - - - - - - 125

LIST OF SYMBOLS

Å	Angstrom
Al	aluminum
Al^{+++}	aluminum ion
Al_2O_3	alumina
$Al_2O_3 \cdot xH_2O$	alumina (hydrated)
$Al(OH)_3$	aluminum hydroxide
B & L	Bausch & Lomb
°C	degrees Celsius
Cl^-	chlorine ion
cm	centimeter
cm^2	square centimeter
CRT	Cathode Ray Tube
Cu	copper
e^-	electron
E	cell potential
F	Faraday constant (96,500 coulombs)
Fe	iron
Fe^{++}	iron ion
Fe_2O_3	ferric oxide (rust)
$Fe_2O_3 \cdot H_2O$	hydrated ferric oxide
ΔG	free-energy change
δ	film thickness
H^+	hydrogen ion
H_2O	water

k	corrosion rate
mm	millimeter
µm	micrometer
n	number of electrons
NaCl	sodium chloride
OH^-	hydroxide ion
O_2	oxygen
PGT®	Princeton Gamma-Tech
pH	standard hydrogen potential
rpm	revolution per minute
SEM	scanning electron microscope
v	volt

ACKNOWLEDGEMENT

First and foremost, the author is indebted to his wife, Jean, not only for encouragement and moral support throughout this project, but also for her editorial efforts in preparing the manuscript. Her contribution is appreciated.

The author also wishes to express his gratitude for the advice and assistance received from Professor Jeff Perkins. Professor Perkins was always available for consultation without being restrictive of individual initiative in this research. His suggestions and comments during the final editing phase were particularly helpful.

Material Science Laboratory Technician, Roy Edwards, deserves special thanks for his assistance during the design and construction of the test tank apparatus and for his untiring efforts to maintain the microscopy equipment. Mr. Edwards is to be commended on his positive, can-do attitude. He significantly contributed to overcoming some troublesome design problems.

I. INTRODUCTION

A. THE EXPLOSIVE-BONDING PROCESS

Explosive-bonding is a process that utilizes the tremendous pressures developed by chemical explosives to force metals together at an oblique angle, thereby resulting in a metallurgical bond between them. By definition, metallurgical bonding results if the cohesive atomic forces of the metals in contact are sufficient to permanently joint them. Joining two metals, whether similar or dissimilar, with cohesive atomic forces is very difficult to achieve in practice. This is primarily due to two factors, 1) atomic interaction implies atomic closeness and 2) all metals have surface films on them in a normal atmospheric environment. Obviously both factors are interrelated but they, at the same time, require independent consideration.

All surfaces have some degree of contour regardless of the method of manufacture. These contours are orders of magnitude larger than the atomic closeness necessary for metallurgical bonding. Therefore some means of resolving the contour differences between the two surfaces must be included in the joining process. The surface films usually are oxides, nitrides or absorbed gases. Some method of dissolving or mechanical cleaning of these films from the surfaces also is necessary.

These two factors are effectively dealt with in many common joining processes. For example, fusion welding, brazing, and soldering are joint processes that effectively disrupt surface films by dissolution or melting while establishing the necessary intimacy by wetting of the molten phases. Likewise roll bonding, friction bonding, and ultrasonic bonding disrupt surface films by severe localized deformation while the surfaces are maintained in contact by high pressure. The explosive-bonding process meets the requirements for metallurgical bonding by the elimination of surface-film material from the interface area and the concurrent development of a very intimate interfacial contact. Each is the result of the high-pressure oblique collison [2]. To better understand how this comes about a more detailed description of explosion-bonding is necessary.

The mechanism of explosive bonding involves high-pressure mechanics and fluid flow. When the collision velocity and angle are controlled within certain limits, the surfaces at the point of collision become fluid and are expelled from the apex of the collision angle. The flow process and expulsion of the surface layer are called jetting. Typically, the plates being bonded must collide with a velocity of 1,000 to 3,000 feet per second. For most metals a collision at those velocities will result in a shock-wave pressure in the surface layers at the collision point of 1.5×10^6 to 4.5×10^6 psi. At such pressures, the yield strength of most materials has been exceeded by about 100 times, and the

materials tend to respond in a highly plastic or fluid manner [4]. Figure 1 [4] gives a stepwise presentation of the probable processes that take place during explosive bonding. The wavy interface is thought to be due to fluctuations in the jet at the collision point. The fluctuations in flow would be caused by the build-up of a hump of material ahead of the collision point as the collision point races across the surface. The build-up of material is due to a slowing of the jet by collision and friction with the metal plates in the narrow gap between them. This in turn interferes with the flow process as the jet flow meets resistance from the mount of material as it increases in size. Eventually the jet flow is momentarily interrupted, and the cladding plate folds over the hump. The resistance to the jet flow is thereby relieved, and the process is free to repeat itself [4]. Generally two manufacturing geometries are used for explosive bonding. These are 1) constant-interface clearance and 2) angular-interface clearance, both of which are shown schematically in Figure 2 [4]. The constant-interface geometry is normally employed with low and medium velocity detonation. For a high-detonation-velocity explosive, the angled-interface geometry is normally necessary to provide the oblique collision and plate velocities for jetting and bonding. An air environment normally exists in the interface during the bonding process.

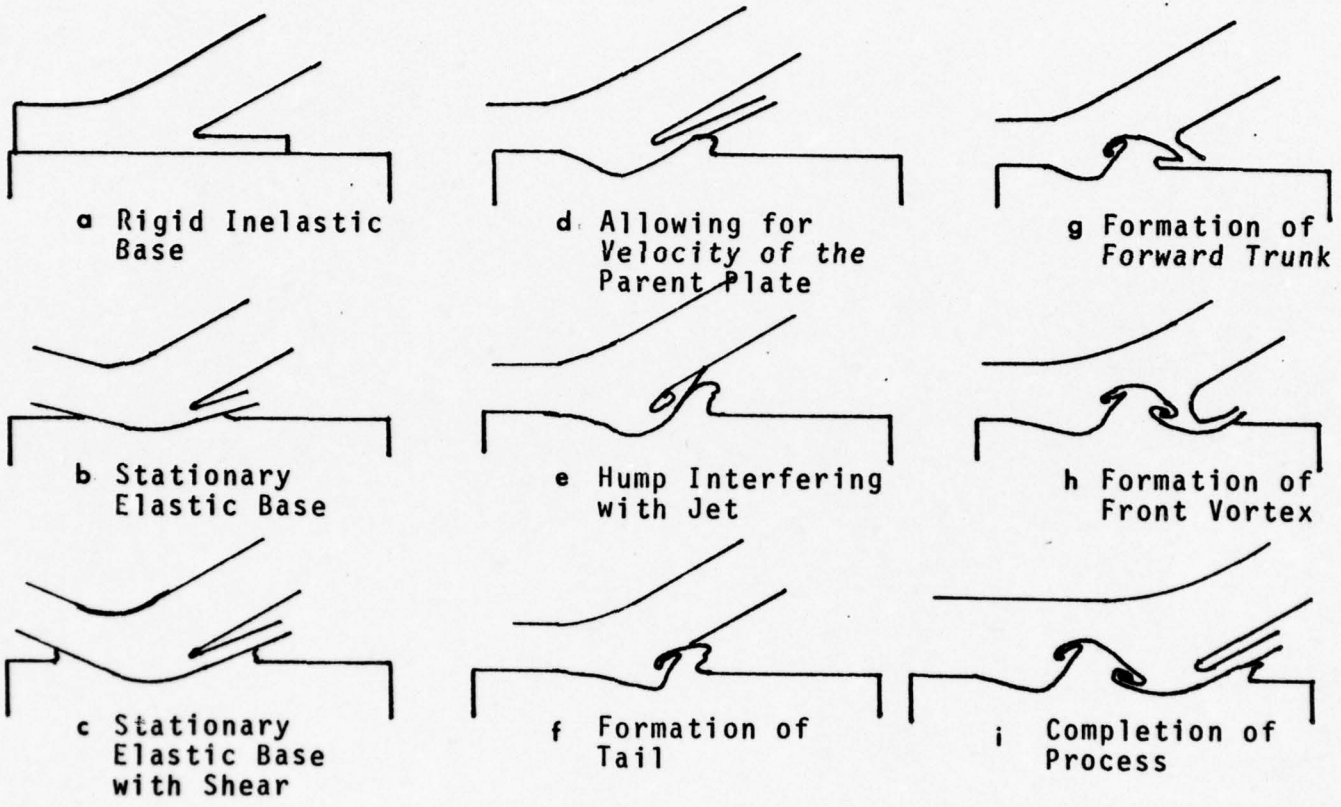

Figure 1. Illustration of rippling phenomenon during explosive bonding.

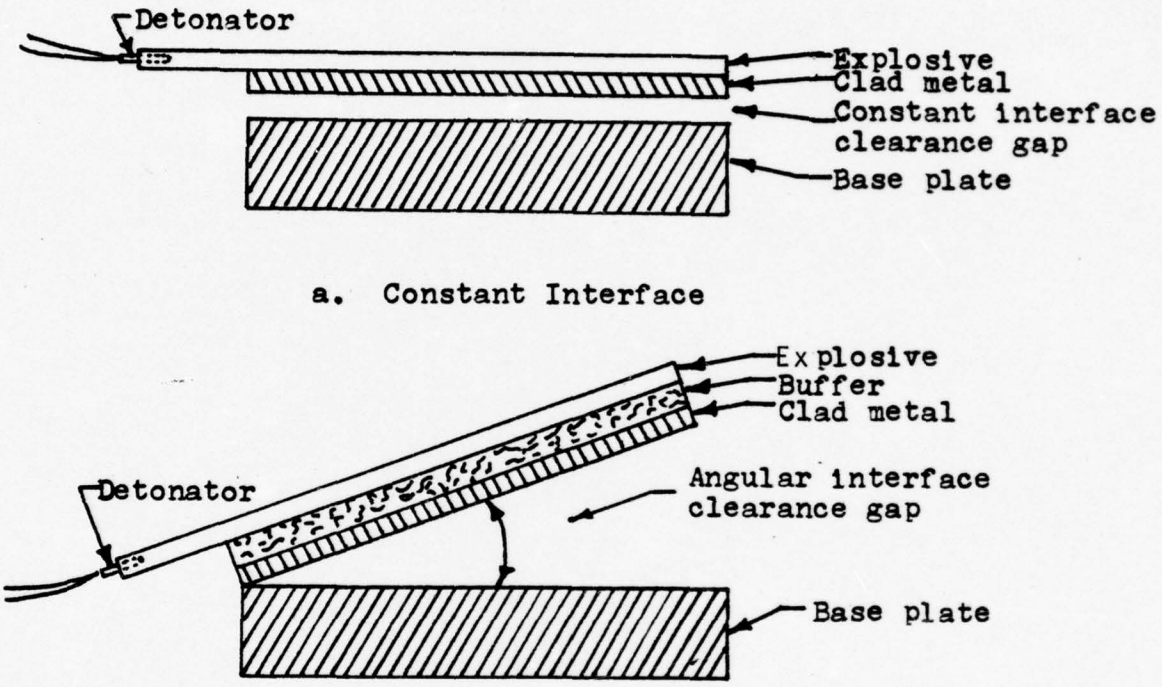

Figure 2. Explosive-metal geometries utilized to accomplish explosive bonding.

B. USES OF EXPLOSIVELY BONDED MATERIALS

The ability to join metals utilizing controlled explosives was first discovered by the DuPont Company in the late 1950's [2]. Over the next several years extensive research was undertaken by DuPont to develop a commercially viable production process out of their discovery. By 1964 they were able to begin manufacturing explosively bonded materials for industrial use. Initially the primary emphasis was on marketing a line of products for use in the chemical processing industry. The extreme environmental conditions under which much of the equipment had to operate in the chemical processing industry had led to the widespread use of bimetallic construction. Pressure vessels and tanks used for settling or decomposition of chemicals were typical examples of bimetallic components. The use of two or more metals in their construction helped balance the cost and strength requirements of a particular application against the need for corrosion resistance. More often than not, the use of other than a single material in construction led to severe constraints on the design and construction of the vessels concerned. Elaborate techniques were needed to ensure tight fitting liners or for ensuring good bonding and coverage of sprayed-on coatings. Optimum operational configurations sometimes were sacrificed for manufacturing requirements. On the other hand, explosively bonded materials were manufactured in standard flat plate and tube stock sizes and then formed through conventional shop methods into the desired vessels.

The ability of explosion-bonded composites to undergo the various industrial forming processes and still maintain their bond created a large demand for them in other industries. One of the more notable applications is the new United States composite coins. These materials have also been widely used in the aerospace, reactor, and cryogenics industries for joining pipes and tubing of dissimilar metals in strong, leaktight bonds. In mid-1966 work began on the development of explosion bonded composites as transition joints between aluminum and steel. The transition joints were in the form of blocks and strips which were obtained by sectioning larger clad plates. Both aluminum and steel could then be attached to the respective faces of the transition pieces by welding. The motivating force behind this research was the desire to join large aluminum bus bars to steel anodes and cathodes in aluminum smelting plants. The resulting couple proved to be very successful. In 1967, it was decided that the difficulties the marine industry faced with mechanical connections between aluminum superstructures and steel hulls could be solved through use of a similar joint.

The advent of radars, communication, and electronic warfare equipment had drastically increased the weight in the superstructure of modern naval vessels. To offset this additional weight most Navies of the World substituted aluminum for steel as the principal structural material above the main deck. Since aluminum cannot be welded directly to

steel, a mechanical connection such as illustrated in Figure 3 was used [20]. Major problems with corrosive deterioration of these joints were common. Even when painted and insulated, random areas soon became exposed to the marine environment where slight working of the structures created localized paint and insulation failures. The presence of a natural mechanical crevice, as well as the significant galvanic potential between aluminum and steel, tended to result in rapid and extensive corrosion in these areas. Therefore the possible use of an explosively bonded joint seemed very promising. Marine joints, unlike the electrical transition joints used in the aluminum smelters, required high strength aluminum and impact resistant steel. After extensive evaluation tests, it was established that optimum product quality was obtained with an aluminum alloy such as 5456 bonded to A516 Grade 55 steel, but employing an interlayer of 1100 aluminum between them. Figure 4 [2T] illustrates the typical triclad product between aluminum and steel plates. Figure 5 [2] demonstrates a typical shipboard installation. This product is marketed as DuPont Detacouple® which is one of a line of products called Detaclad. Detacouple® was initially adopted by the United States Navy on an experimental basis as a repair for sections of deteriorated mechanical joints. More recently it was incorporated into the basic design and production of the new Spruance class destroyer, the new Patrol Frigate and LHA's.

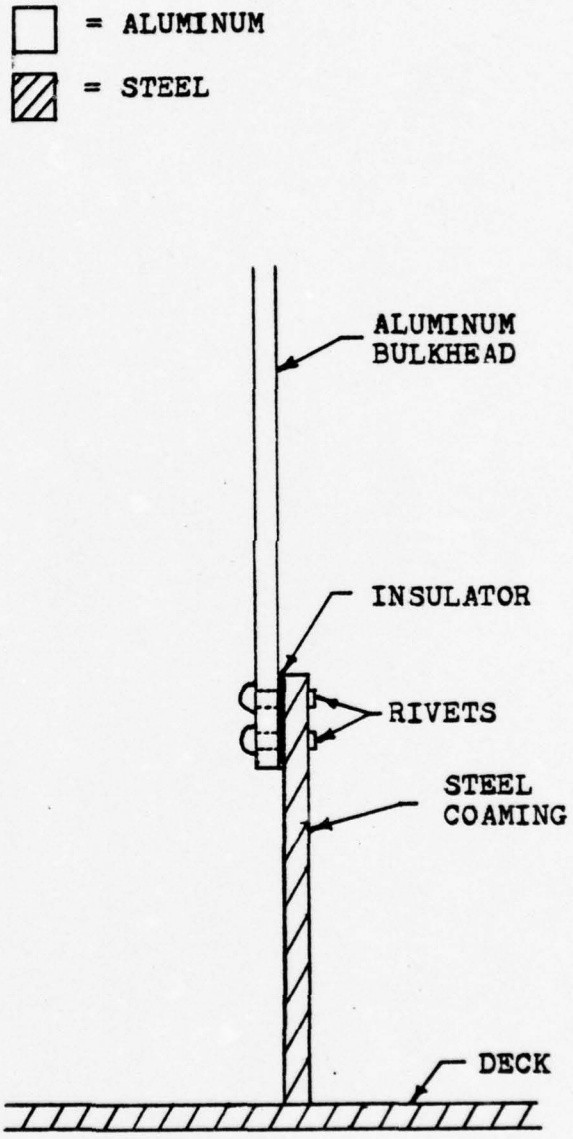

Figure 3. Mechanical fastening technique.

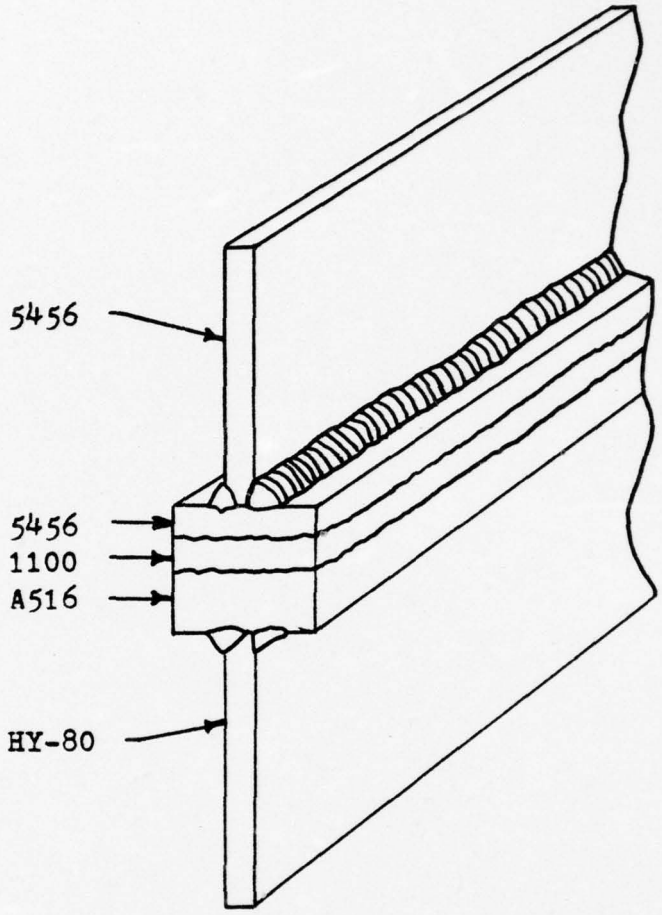

Figure 4. Typical explosively bonded joint with webs.

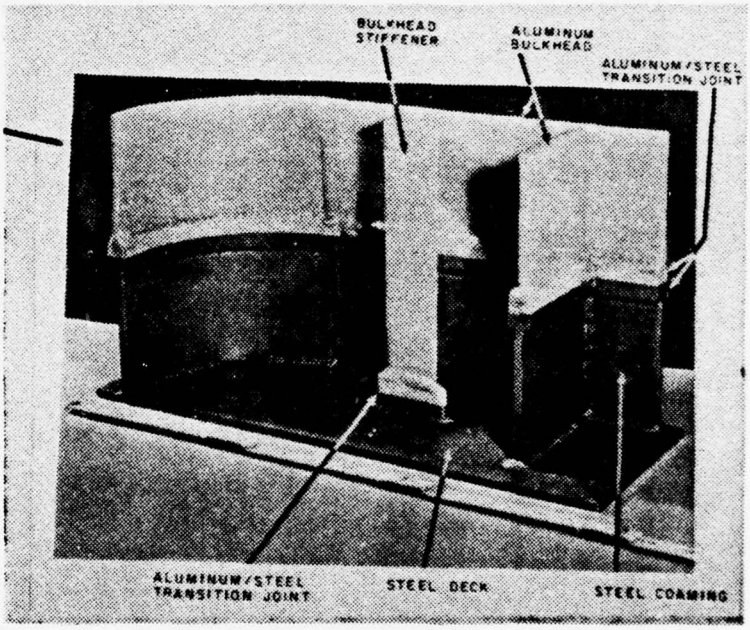

Figure 5. Typical aluminum superstructure and steel deck connection demonstrating the use of welding transition joints.

C. PREVIOUS TESTING

Testing of Detacouple® transition joints to date has been primarily oriented toward proving their mechanical properties with only limited research into corrosion. This is probably due in part to the discovery that the major factor for the mechanical joint failures was crevice corrosion rather than galvanic attack. By substituting Detacouple® joints the natural crevice was removed thus reducing the probability of poor service performance due to corrosion. The mechanical properties, on the other hand, were somewhat of an unknown due to the newness of the product. Mechanical checks such as tensile testing, shear testing, fatigue testing, and hardness testing also would normally be included in a quality control program so these parameters needed to be well established. DuPont, in a study undertaken in conjunction with the development of Detacouple® [2], tested the actual, as welded, tensile strength of the composite to be 13,500 psi. Based on this, a four-to-one area ratio was sufficient to provide the transition strip with slightly greater strength than a 5456 aluminum panel welded to it. Other tests in their study demonstrated that the transition joints had much more than adequate shear, impact, and crack propagation resistance [2]. During evaluations under fatigue loading, the explosion-bonded strip far exceeded the cycles to failure of the traditional mechanical joint.

The major corrosion study of Detacouple® transition joints to date was undertaken by the Naval Ship Research

and Development Center, at Harbor Island and Wrightsville Beach, North Carolina, during 1969, 1970 and 1971 [21]. The tests consisted of exposing samples of the bonded material with attached webs to the marine atmosphere for one and two years. Microscopic examination revealed that the aluminum initially had a slight penetration at the interface as anticipated. However, rather than acting as a point of high ion concentration and accelerating corrosion, the area quickly filled with corrosion product. The initial corrosion product sealed off the aluminum-steel interface from the corrosion environment and reduced the corrosion to an almost negligible rate. Over the initial three months, corrosion penetrated .027 inches into the aluminum at the interface. During the next nine months the penetration increased by only .006 inches; and after 27 months total exposure, the maximum penetration was only .042 inches. DuPont confirmed these basic results utilizing accelerated salt spray tests (ASTM B117-57T)[2]. In-service testing is also in progress on several ships of the United States Navy, but as yet no results have been published.

All of these tests have been macroscopic in nature. The present study was undertaken to provide a better characterization of the actual corrosion taking place and to again verify previous findings. To do this microscopic techniques were utilized.

D. ELECTROCHEMICAL BACKGROUND

Most metals in their natural state exist as compounds (oxides, sulfides, etc:). This is their thermodynamically stable state. We utilize metals for the most part only after they have been processed. When they are again exposed to a natural environment, they tend to revert to their natural state by corroding to form compounds. Every metal requires certain environmental conditions before its deterioration can proceed. To determine which environments promote corrosion on which metals, the laws of thermodynamics must be considered. The laws of thermodynamics indicate that for a reaction to proceed naturally, the reactants must experience a negative free-energy change (ΔG). For electrochemical reactions:

$$\Delta G = -nFE$$

where n is the number of electrons involved in the reaction, F is the Faraday constant, and E is the cell potential. The reaction is feasible when the cell potential is positive. Cell potentials are determined by considering separate anode and cathode reactions. Considering the anode and cathode reactions separately allows us to compare the potential difference between each metal and its ions in solution. Some typical half cell potentials are summarized in Table 1 [11].

Utilizing Table 1 the cell potentials for aluminum and steel in sea water solution can be estimated. Sea water is

Table 1. Standard oxidation-reduction potentials

	Volts*
$Au = Au^{+++} + 3e$	+1.498
$O_2 + 4H^+ + 4e = 2H_2O$	+1.229
$Ag = Ag^+ + e$	+0.799
$Fe^{+++} + e = Fe^{++}$	+0.771
$O_2 + 2H_2O + 4e = 4OH^-$	+0.401
$Cu = Cu^{++} + 2e$	+0.337
$2H^+ + 2e = H_2$	+0.000
$Ni = Ni^{++} + 2e$	-0.250
$Fe = Fe^{++} + 2e$	-0.440
$Cr = Cr^{+++} + 3e$	-0.744
$Zn = Zn^{++} + 2e$	-0.763
$Al = Al^{+++} + 2e$	-1.662
$Na = Na^+ + e$	-2.714

*Volts versus normal hydrogen electrode at 25 C.

slightly alkaline; therefore the most likely reactions would be:

$$Fe \rightarrow Fe^{++} + 2e^{-}$$
$$Al \rightarrow Al^{+++} + 3e^{-} \qquad \text{Oxidation}$$

$$O_2 + 2H_2O + 4e^{-} \rightarrow 4OH^{-} \qquad \text{Reduction}$$

$$E(\text{Steel}) = E(O_2/OH^{-}) - E(Fe/Fe^{++})$$
$$= +0.401 - (0.440)$$
$$= +0.841v$$
$$E(\text{Aluminum}) = E(O_2/OH^{-}) - E(Al/Al^{+++})$$
$$= +0.401 - (-1.662)$$
$$= +2.063v$$

Since both cell potentials are positive, the free energy changes for both reactions would be negative and both reactions are feasible (see note).

While the reactions are possible, the environment should be examined to determine their likelihood. Testing of the Detacouple samples in this study was accomplished by periodically spraying them with artificial sea water. For purposes of discussion, variations in environment during testing can be put into four distinct categories [25]:

1) Dry air
2) Moist atmosphere
3) Wet atmosphere
4) Immersed

The dry air exposure considerations are necessary because each sample was usually exposed to room air conditions for a minimum of one hour prior to being placed into the test tank

environment. Deterioration during this time would proceed by purely chemical reaction with gaseous agents, such as atmospheric oxygen, hydrogen sulfide, etc. The growth of a thin oxidized layer will be maximum during the first few minutes after sanding, and will nearly cease after two to three hours. The layer formed would be expected to range in thickness from 10 to 100Å and not be visible to the naked eye. Figure 6 [25] shows the characteristic decrease of corrosion in dry air with time.

Once the samples are placed within the atmosphere of the testing tank they repeatedly experience the other three environmental categories. Before going into the specifics of each category, some characteristics of the samples should first be examined. Detacouple® is made of bonded aluminum and steel so that in the presence of an electrolyte there is a possibility of galvanic attack. For this situation, the basic equations for single-metal corrosion processes do not change, but the relative rates at which they proceed are different. Bimetallic couples in the presence of a conductive solution tend to accelerate corrosion of the more active metal and retard corrosion on the more noble. Table 2 [7] indicates the relative standings of various metals in the galvanic series in sea water. Aluminum is more active than steel and would therefore experience accelerated corrosion due to a couple. The increased oxidation would normally be most pronounced at the junction of the two metals; and if the electrolyte is highly conductive,it can be sustained farther away as well. When the conducting solution

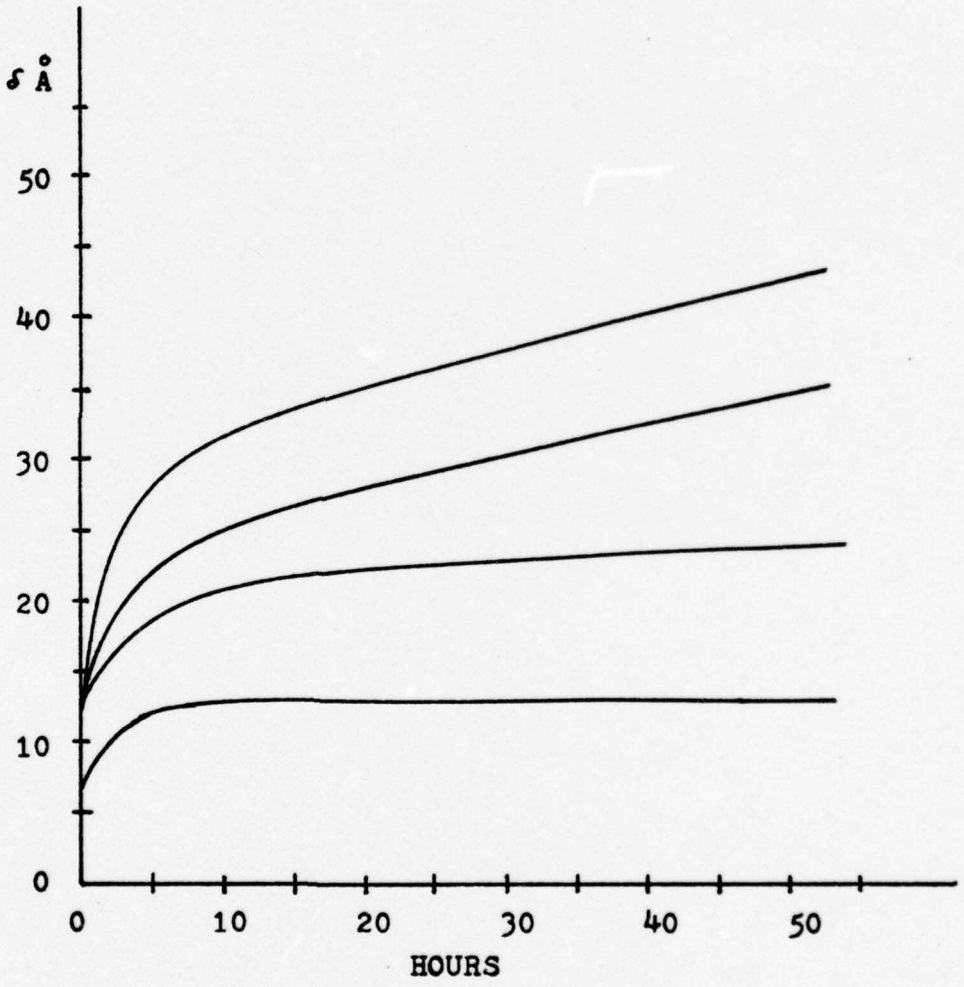

Figure 6. Kinetics of the growth of oxide films on various metals at room temperature in oxygen or dry air.

Table 2. Galvanic series of some commercial metals and alloys in seawater

↑	Platinum
	Gold
Noble or	Graphite
cathodic	Titanium
	Silver
	Chlorimet 3 (62 Ni, 18 Cr, 18 Mo)
	Hastelloy C (62 Ni, 17 Cr, 15 Mo)
	18-8 Mo stainless steel (passive)
	18-8 stainless steel (passive)
	Chromium stainless steel 11-30% Cr (passive)
	Inconel (passive) (80 Ni, 13 Cr, 7 Fe)
	Nickel (passive)
	Silver solder
	Monel (70 Ni, 30 Cu)
	Cupronickels (60-90 Cu, 40-10 Ni)
	Bronzes (Cu-Sn)
	Copper
	Brasses (Cu-Zn)
	Chlorimet 2 (66 Ni, 32 Mo, 1 Fe)
	Hastelloy B (60 Ni, 30 Mo, 6 Fe, 1 Mn)
	Inconel (active)
	Nickel (active)
	Tin
	Lead
	Lead-tin solders
	18-8 Mo stainless steel (active)
	18-8 stainless steel (active)
	Ni-Resist (high Ni cast iron)
	Chromium stainless steel, 13% Cr (active)
	Cast iron
	Steel or iron
	2024 aluminum (4.5 Cu, 1.5 Mg, 0.6 Mn)
Active or	Cadmium
anodic	Commercially pure aluminum (1100)
	Zinc
↓	Magnesium and magnesium alloys

does not cover the interface of the bimetallic couple, each metal corrodes independently. Localized single-metal electrochemical corrosion occurs on each metal surface whenever there is sufficient electrolyte.

In the last three environmental categories, galvanic attack at the bimetallic interface and localized electrochemical corrosion can occur simultaneously depending on the location on the specimen and distribution of the electrolyte. The distinction between the categories is mainly in terms of the rate at which processes take place and of what happens to corrosion products once they are formed.

In the category of moist atmospheric corrosion, relative humidity is less than 100%. Corrosion proceeds under an extemely thin, invisible film of electrolyte formed on the surface by capillary action, adsorption, chemical condensation, or partial drying of a thicker film. The film thickness is generally on the order of 100Å to 1μm in this category. With this thin film of electrolyte the rate of corrosion is very rapid due to the nearly unimpaired diffusion of oxygen. Also, the radius of activity of the microcells is very small. The initial products of the anodic reaction (metal ions) and the cathode reaction (OH^- ions) subsequently react within the electrolyte directly adjacent to the metal surface, leading to the formation of several hydrous and anhydrous oxides (for both the aluminum and the steel), which tend to adhere to their respective surfaces far better than they would during immersion corrosion.

Category three is wet atmospheric corrosion. The electrolyte thickness here ranges from 1μm to 1 mm and is normally in the form of droplets either from additional condensation from the moist atmospheric phase or from some drying after immersion. This conforms to 100% relative humidity. This category is distinguished from the moist atmosphere mainly by a slight reduction in corrosion rate with the main reason for the decrease being poorer oxygen diffusion through the thickened film. There is also relatively less product adhesion to the surface.

Category four includes any electrolyte film thickness over 1 mm and is considered effectively total immersion. In these experiments, the duration of "immersion" for each cycle while in the test tank is considered to be quite brief compared to the other two categories (categories two and three). One group of samples was immersed for an estimated two seconds out of a two-minute cycle, while another group was immersed for about five seconds out of a five minute cycle. Besides this time difference, the category four environment leads to a further slight decrease in the rate of reaction due to lower oxygen in solution at the metal surface. Also the subsequent products of the surface reaction tend to be carried away.

Figure 7 [25] summarizes the relationship between the rate of corrosion and the moisture film.

Other important facets of the corrosion process are the roles of passivation, aggressive anions, and polarization.

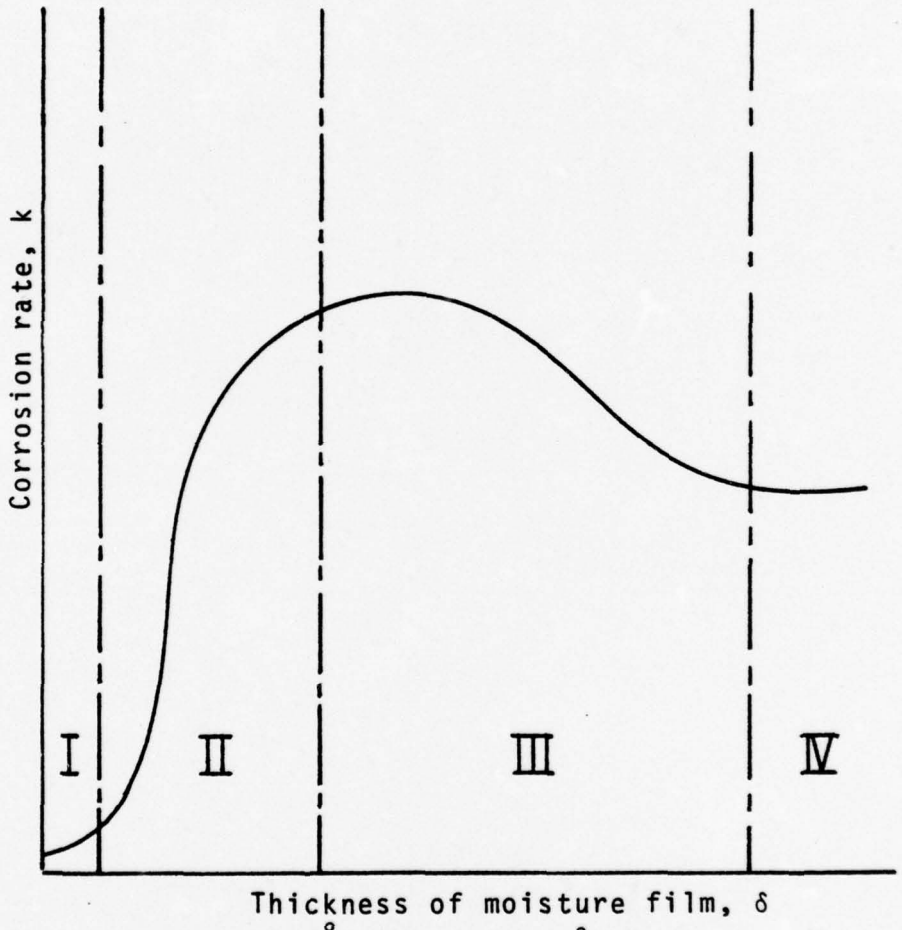

I-δ = 10 to 100 Å; II-δ ≈ 100 Å to 1 micron;
III-δ ≈ 1 μ to 1 mm; IV-δ > 1 mm.

Figure 7. Dependence of atmospheric corrosion on thickness of the moisture film on the metal surface.

A metal is said to be passive in an environment if it shows a very low corrosion rate, when thermodynamically it would be expected to corrode rapidly. Passivation is generally associated with oxidizing media (high, positive potential) and the formation of thin protective oxide films [18, 23]. If a metal can be oxidized to an oxide that is stable in the electrolyte, then the metal is passivated. Passive films have some electrical conductivity. They are not insulators. Consequently the passive film can only protect the underlying metal under comparatively low potential conditions. If the potential increases, then the current also increases by a rise in anodic action. Figure 8 [23] shows a typical anodic polarization curve for a specimen exhibiting passivity. Potential increases in the region between C and D do not lead to increased anodic activity while increases above D once again lead to increased corrosion. If the oxide film is soluble in the electrolyte, the corrosion rate will be controlled by the growth of the film. The film growth is inversely related to the resistance of the film. When the film thins by going into solution, the rate of corrosion and, hence, film growth increases, and, conversely, when the film thickens, the corrosion and growth rates decrease. At equilibrium the oxide layer is maintained at a constant thickness.

Passivity cannot be easily established nor maintained in the presence of aggressive anions such as Cl^-. As the concentration of such ions is increased, they compete with the oxidizing species and become incorporated into the film.

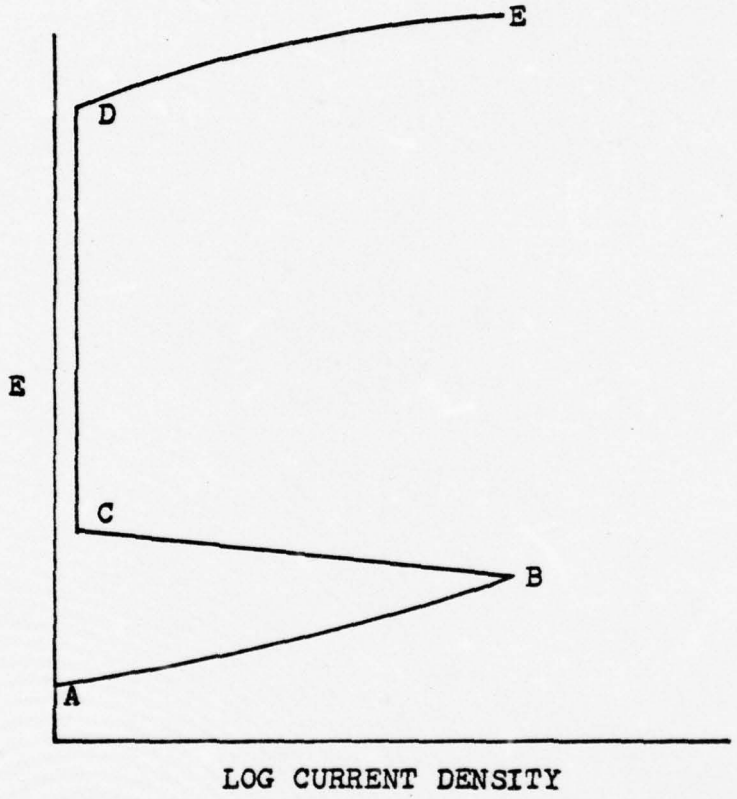

Figure 8. Anodic polarization curve for a specimen exhibiting passivity, determined potentiostatically.

This produces lattice defects, thereby reducing the resistivity of the oxide. The effect of the decreased resistance is an increase in current density in the passified range of potentials. Likewise the potential level at which passification begins is raised while the overall range of passive potentials decreases. These influences are graphically illustrated in Figure 9 [23].

Polarization is defined as a change in electrode potential as current flows to or from it (anode or cathode). As polarization increases, the rate of corrosion decreases. There are basically three reasons for polarization: activation, concentration, and IR-drop. Activation polarization is the result of one step in a reaction sequence at either the anode or cathode being slower than the others and thereby controlling the overall rate. The term activation is derived from the need for a certain quantity of activation energy before a particular step in a chain can occur. This type of polarization takes place at the interface between the metal and the electrolyte.

Concentration polarization, on the other hand, is a function of the electrolyte. In this case, the electrochemical reactions are controlled by the diffusion rate within the electrolyte. The species to be reduced must arrive at the metal surface in sufficient quantity to sustain a given reaction rate. Concentration polarization generally predominates when the concentration of reducible species is small (e.g. dilute acids, aerated salt solutions) [7].

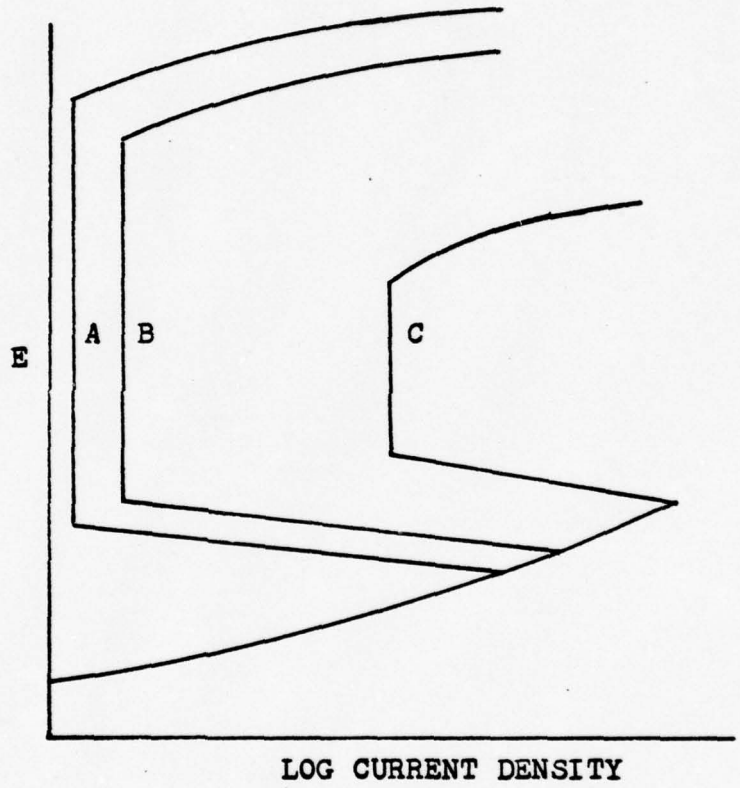

Figure 9. The effect of chloride ion upon the anodic polarization curve for a metal that exhibits passivity.

A. No chloride ions present.
B. A low concentration of chloride ions.
C. A high concentration of chloride ions.

IR-drop polarization includes potential drop through a portion of the electrolyte surrounding the electrode, through any oxide type film on the electrode surface, or both.

The ultimate corrosion rate of any metal or combination of metals depends then not only on the environmental conditions but also on the existence of aggressive anions, formation of passivating films, polarization dynamics, and all their possible interactions.

E. CORROSION MODEL

Figure 10 is a schematic presentation of a sample with its moisture film and probable reactions. The sample was initially devoid of protective coatings such as greases or paints, with the exception of the previously discussed thin film formed in dry air. Upon entering the test tank the following occurs:

$$1)\quad Fe \rightarrow Fe^{++} + 2e^{-}$$

$$2)\quad Al \rightarrow Al^{+++} + 3e^{-}$$

$$3)\quad O_2 + 2e^{-} + H_2O \rightarrow 4OH^{-}$$

Once a sufficient number of ferrous ions and hydroxide ions are formed they further react to form hydrated ferric oxide (rust), with a chemical composition approximating $2Fe_2O_3 \cdot 3H_2O$, as follows:

$$4Fe^{++} + O_2(g) + (4+2x)H_2O \rightarrow 2(Fe_2O_3 \cdot xH_2O)(s) + 8H^{+}$$

Likewise, aluminum ions and hydroxide ions react to form hydrated alumina ($Al_2O_3 \cdot H_2O$) or aluminum hydroxide ($Al(OH)_3$).

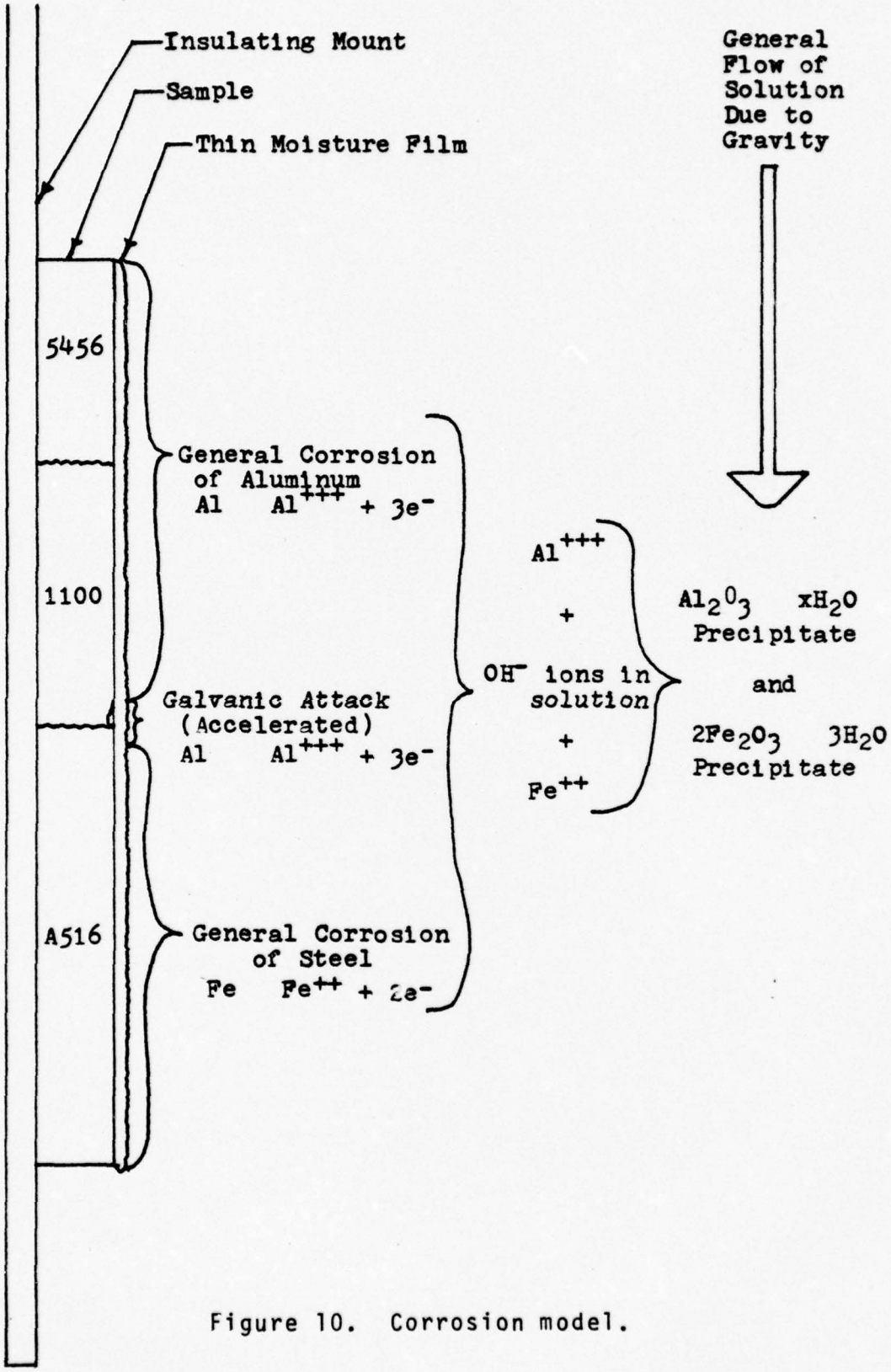

Figure 10. Corrosion model.

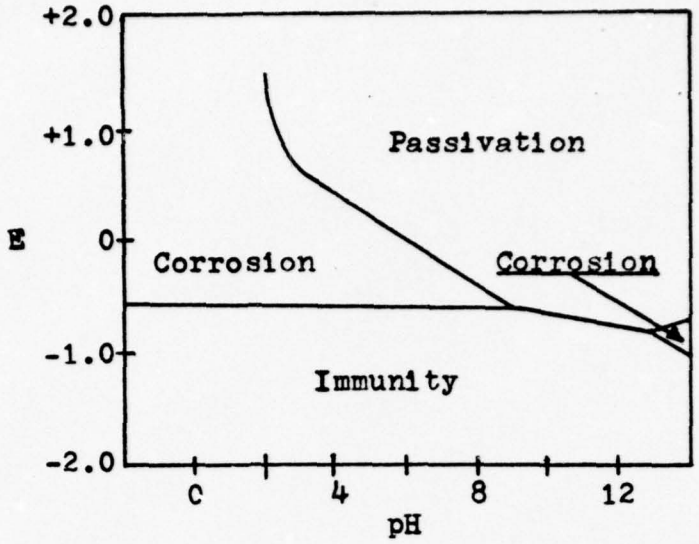

Figure 11. Pourbaix diagram shows theoretical conditions for corrosion of metallic iron.

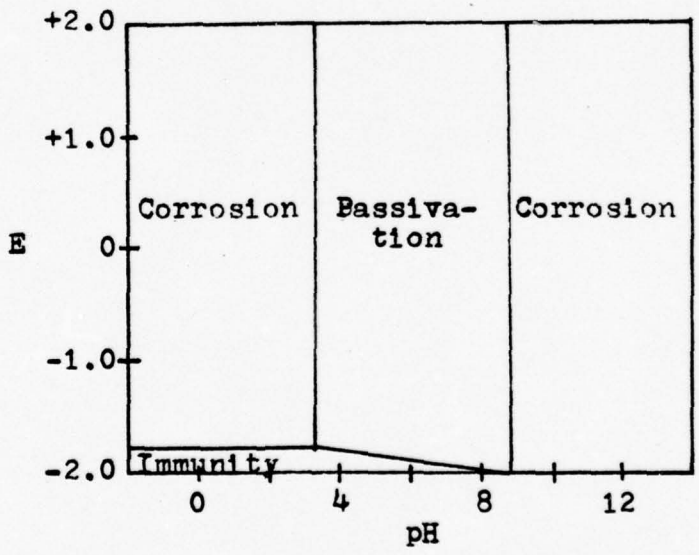

Figure 12. Pourbaix diagram shows theoretical conditions for corrosion of metallic aluminum.

The reactions are:

$$2Al(s) + 3/2\ O_2(g) + xH_2O \rightarrow Al_2O_3 \cdot xH_2O$$

or $$Al^{+++} + 3OH^- \rightarrow Al(OH)_3$$

Both then precipitate to the surface of the sample to form protective coatings. Figures 11 and 12 show simplified Pourbaix diagrams [22] for iron and aluminum respectively. Recalling the oxidation reduction potentials that were calculated for Al^{+++} and Fe^{++}, it can be seen that passivation is likely within the pH range of the test environment.

Complicating the model is the Cl^- ion formed naturally in solution by the major constitutent of sea water, NaCl. As mentioned the Cl^- ion tends to reduce the resistance to dissolution of the oxide layers. However, aluminum hydroxide becomes progressively more difficult to dissolve after it has set for a period of time, so that, a general thickening of the protective layer could be anticipated to offset the tendency to dissolve in the presence of Cl^- ion. Ferric oxide, however, is less insoluble. Therefore it could be anticipated that a passivation layer would never grow sufficiently on the steel while in the Cl^- environment, and the steel section of the samples would continue to rust.

Gravity also plays an important role during the corrosion process in the present situation. Since the aluminum half of the bimetallic couple is located physically above the steel half, a certain amount of hydrated alumina could be expected to precipitate onto the steel near the interface.

The various thicknesses of electrolyte experienced during each cycle should contribute only to the rate of oxide formation but not to the end results. If the length of immersion per cycle were significantly increased then a reduction or loss of passivation would likely occur (assuming this was done at the beginning of the experiment).

It should be understood that the model presented here is a very simplified one. Many other reactions occur and several other factors have an affect, but the fundamental reactions and results predicted should be reasonably accurate.

II. EXPERIMENTAL STRUCTURE

A. APPARATUS

The purpose of this investigation was to study and characterize the corrosion processes on Detacouple® joints exposed to the marine environment. Care was taken to use an experimental setup that would yield not only reproducible results but also utilize standardized and accepted testing techniques. The American Society for Tests and Materials (ASTM) standard method of salt spray testing, designation B117-73, was used for reference during the test assembly construction.

1. Tank Assembly

The tank used for this experiment was constructed from Marine grade plywood and painted with a non-reacting water sealing paint. Its dimensions were 127 cm (50 in) long, 76.2 cm (30 in) wide, and 31.75 cm (12.5 in) deep. Artificial sea water was maintained to a level of about 4.5 cm (1 3/4 in)(approximatley 15 gallons) in the bottom of the tank at all times. A baffle plate above the water level separated the tank into two chambers which allowed sample exposure variations while assuring simulitude of spray water makeup. Plexiglass covered the tank to reduce evaporation water losses and at the same time permit inspection while spraying was in progress.

Within each chamber a spoked, stainless steel rim 50.8 cm (20 in) in diameter and 15.26 cm (6 in) wide rotated in a horizontal plane. Stainless steel shafts extended from the bottom of the tank through the centers of the spokes in the rims, through bearings in the top of the tank to pulleys which were driven by synchronous motors. Figure 13 shows the test tank with one of the rim assemblies removed and set on top.

Test samples were placed on each rotating rim with plexiglass holders. These holders allowed installation and removal of samples without interrupting the exposure process. They also provided insulation between the sample, rim, and adjacent specimens. Rubber cement was utilized to mount the samples to their holders. Figure 14 shows a close up view of a rim assembly with a sample installed.

Each chamber of the test tank also contained a spray nozzle mechanism. The nozzle assembly extended from the bottom of the tank and sprayed continuously as the samples rotated by it. The nozzles were designed to minimize the direct impingement velocity of the spray mist on the samples. A single stream of sea water at very low pressure exited from the center of the nozzle while two jets of air, at 3 to 5 psi, were directed at 45° angles.

The net effect of this design was to flatten out the water stream and create a fine vertical line of mist much like that provided by a normal spray painting gun. Figure 15 shows a rim assembly installed in its chamber with a nozzle assembly in the upper right chamber corner.

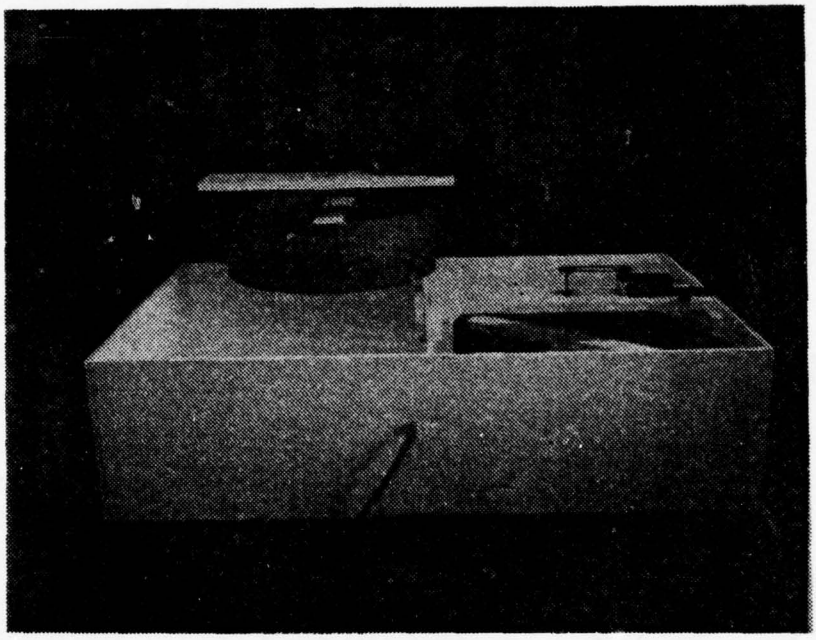

Figure 13. Tank with one rim assembly removed and placed on top.

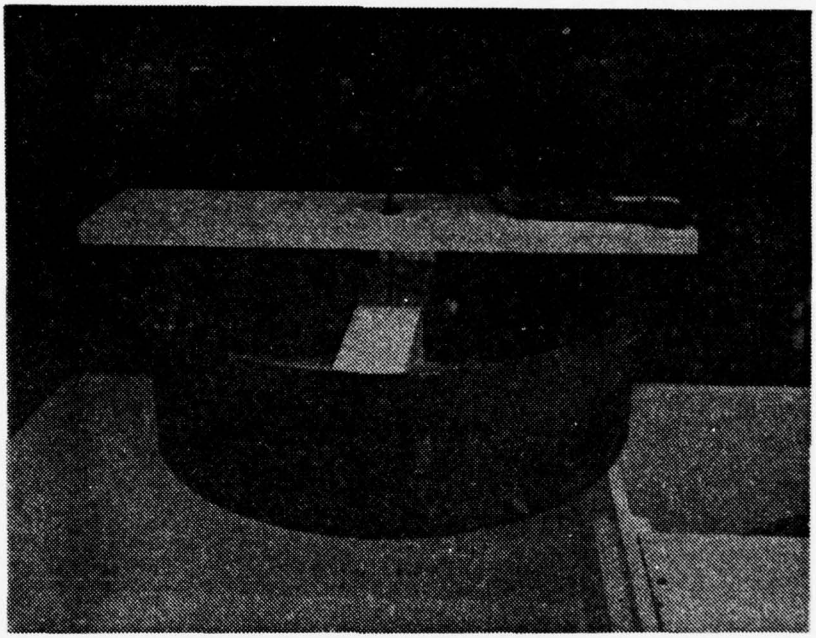

Figure 14. Close-up of rim assembly and installed sample.

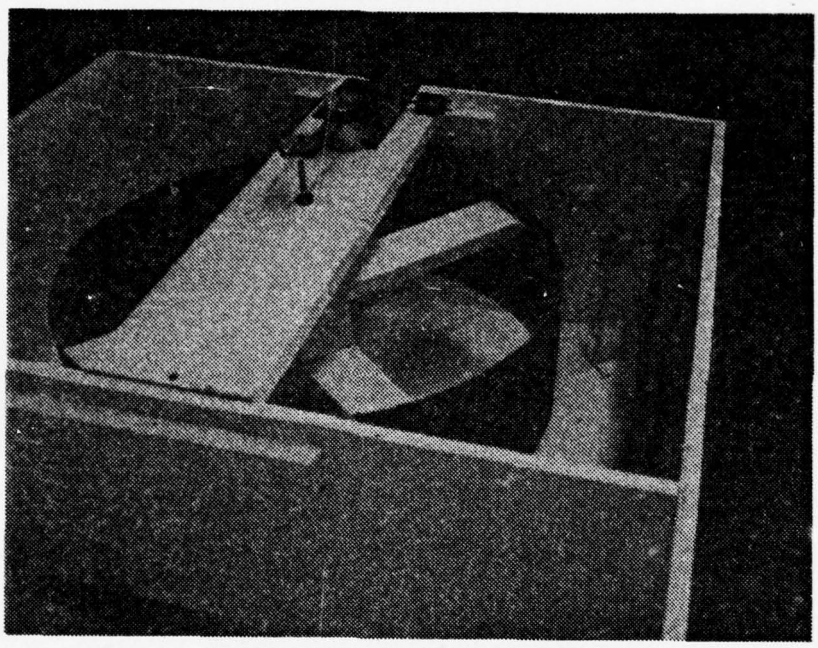

Figure 15. Rim assembly and nozzle installed in chamber.

2. Microscopes

Three different microscopes were used in performing the analysis of the corrosion process. For very low magnification studies a Bausch and Lomb 7x to 30x binocular microscope was utilized. Low magnification viewing helped to establish a basic standard surface finish on prepared samples. In the intermediate range of magnification, 80x - 800x, some studies were done on a Bausch and Lomb Dynazoom Bench Metallograph. This instrument has a very limited depth of focus and therefore was used only to view polished samples prior to testing. Examination of the wavy interface and the vortex area of the waves was performed with the bench metallograph.

The bulk of microscopic research during this study was accomplished with the Cambridge Model S4-10 Scanning Electron Microscope (SEM) and attached Princeton Gamma-Tech PGT-1000 X-ray Analyzer, Figure 16. The scanning electron microscope utilizes a condensed beam of electrons in much the same way as a light microscope uses light rays. Electrons are emitted from an electron gun and pass through a series of electromagnetic condensing lenses. These lenses direct the beam in a scanning fashion over the surface of the specimen. When the electrons strike the sample, some are backscattered (reflected), and others cause secondary electron emissions. The specimen is tilted in such a way that some of the backscattered and secondary electrons collide with a collector. The signal from the collector is coordinated with the scan of the angle and is displayed after processing on a

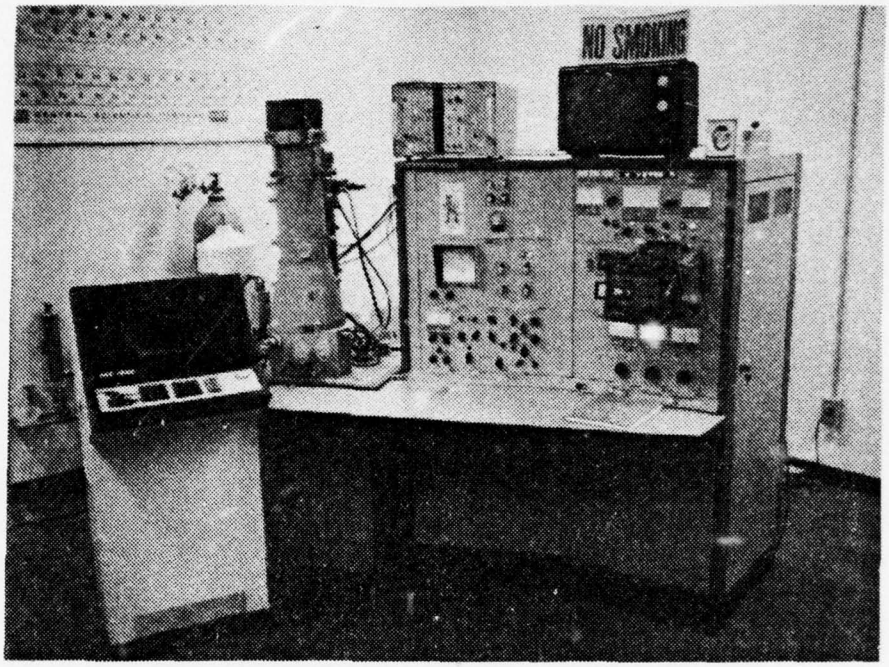

Figure 16. Cambridge Model S4-10 Scanning Electron Microscope (SEM) and attached Princeton Gamma-Tech PGT-1000 X-ray Analyzer.

long-persistence visual display cathode ray tube (CRT). Magnification is achieved by reducing the size of the scan on the specimen while holding the size of the image on the CRT the same.

The SEM is an excellent tool for this type of research because of its great depth of field and many built-in control features. The biasing mechanism was particularly useful in this study. It biased the collector against the secondary electrons. By utilizing this, the CRT image became a representation of backscattered electrons. The number of electrons backscattered from any specific location on a specimen was directly related to the density of the specimen material at that location. While examining the area immediately adjacent to the interface, using high magnification, it was often necessary to resort to this control to separate the more dense steel from the lighter aluminum.

The PGT-1000 is an energy-dispersive x-ray analyzer. As the atoms of the specimen are excited by the incoming electrons, some x-ray emissions also occur. Atoms of each atomic element emit x-ray quanta of characteristic energy. The x-rays from the specimen impinge on a silicon detector which in turn creates amplified pulses. The amplified pulses are then sorted according to pulse height (energy) and displayed on a CRT screen as the number of pulses of a given energy (represented by the relative height of lines across the screen) versus energy.

This system is very quick but normally is only used for qualitative analysis of specimens. A major drawback to its usefulness in this research was its inability to identify compounds and elements below about eight on the atomic chart. Even with these drawbacks it was still useful for checking elemental consistencies of corrosion product formations.

B. PROCEDURES

The Detacouple samples used in this experiment were machined from 45.75 cm (18 in) long bars of 2.54 cm (1 in) wide triclad consisting of 6.35 mm (¼ in) of 5456-H117 aluminum alloy, on 9.53 mm ($\frac{3}{8}$ in) of 1100 aluminum alloy, on 19.05 mm ($\frac{3}{4}$ in) of ASTM A516 grade 55 steel. This material conforms with both military and DuPont specifications [5,6] and was supplied by Naval Ship Research and Development Center, Annapolis Laboratory, Annapolis, Maryland. Each specimen was machined to ensure that the bond profile exposed in the test tank would be identical to the profile that would see in-service exposure. After machining, the samples were the depth of the triclad, 3.49 cm (1 $\frac{3}{8}$ in), with 1.27 cm (½ in) width, and 6.35 mm (¼ in) thickness. Care was taken at this point to eliminate any sample that could be considered abnormal, i.e., unusually large wave vortices, voids, or deep machining grooves. As a further step to ensure uniformity, all specimens were given a standard surface finish. Belt sanding with a #50 grit size sand paper was used in this case because the resulting grooves were similar in size to those that would be left during the manufacturing of the joints. All

sanding was done from the steel section toward the aluminum section to avoid wiping the softer aluminum over the interface thereby obscuring the interface reaction. Each sample was then given an identification number and mounted on a plexiglass holder. Once on a holder the specimens were placed on one of the two specimen wheels for predetermined periods of exposure.

All tests were run with artificial sea water that was prepared in the laboratory just prior to the initiation of the experiment [19].

During the exposure runs each sample wheel rotated at a different speed. This was an attempt to see if there were any correlations between exposures to spray, duration of exposure and the extent of corrosion. In this study one wheel rotated at a constant 1/5 rpm and the other rotated at 1/2 rpm. This results in 12 and 30 spray exposures per hour respectively.

The length of time in the test tank during the experiment ranged from 30 minutes to 9 weeks. During this time span, periodic checks were made on the sea water for conductivity and pH. Conductivity was maintained between 41.0 and 45.0 millimhos and pH was maintained between 7.6 and 8.3. This normally required the addition of distilled water to compensate for evaporative losses and occasional added aerations. Aeration was accomplished by bubbling low pressure air through the tank water. Temperatures during the testing

period ranged from a low of 20 1/2°C to a high of 23°C with the predominant temperature being 21°C.

Samples were removed frequently during the first two days and weekly thereafter. In each case a sample was removed from each wheel so that they could be compared. Samples were immediately rinsed in distilled water when they were removed from the tank and then air dried. After they had dried sufficiently, they were carefully trimmed to fit on a 1/2-inch diameter holder used in the SEM. Excessive heating was avoided during this process so that the surface formation would not be damaged.

III. RESULTS AND DISCUSSION

A. UNEXPOSED SAMPLE

To understand the corrosion that takes place during exposure, a clear picture of the bond interface profile is necessary. For purposes of discussion the term exposure will refer only to the time in the testing tank and will exclude the air environment before and after that period. Therefore unexposed samples would be those samples which have not been in the test tank.

In order to bring out some salient features, an unexposed sample was mounted in bakelite, sanded with a series of fine grit sandpapers and given a final finish on a diamond impregnated polishing wheel. While this procedure was relatively quick and easy, it had a major drawback. The 1100 aluminum in the center of the sample is much softer than either the 5456 aluminum or ASTM A516 steel and, therefore, was preferentially removed. A perceptible ridge at the respective interfaces resulted, with the 1100 aluminum being slightly lower than either of the other metals. This was not a serious handicap to viewing with the binocular microscope but made extensive interface examination on the bench metallograph almost impossible.

Figure 17 is a binocular photomicrograph of a 125 mm-square segment cut from the center of a standard test

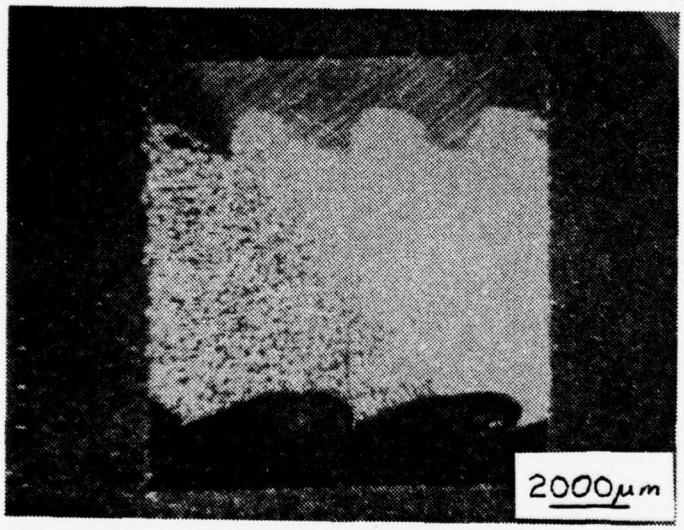

Figure 17. 5.5x binocular photomicrograph of a polished 12.5 mm-square segment of standard test sample (5456 Al-top, 1100 Al-middle, ASTM A516 Steel-bottom).

sample and prepared as described. Both bonds were accomplished with the explosion process proceeding from left to right. A significant difference in the bond profiles is readily observed in this picture. These profiles were found to be typical for the Detacouple® triclad. The bonding procedures for this material call for the 1100 aluminum to be bonded to the 5456 alloy base and then for that composite to be bonded to the steel. The result of this sequence is observed in Figure 17. Comparing this to Figure 1 it can be seen that the aluminum to aluminum interface tends to be made of waves that are relatively high with flat crests, tails, and short forward trunks. On the other hand, the steel-to-aluminum profile shows a complete lack of a tail, a lower extended rolling crest, and an extreme front trunk and vortex complex. Almost all the voids observed in the Detacouple® joints were in the vortex areas. Since the steel and aluminum interface represents the primary area for probable galvanic attack, the remainder of this discussion will concentrate on it exclusively.

Figure 18 is an enlarged picture of the steel-aluminum interface profile utilizing the same sample. Particularly noteworthy here are the sections of material that have neither the rough eroded texture of the aluminum nor the smooth surface of the steel. These areas have a gray appearance in the figure and are located in the interface and vortices. This material is actually melt from the metal surfaces, formed during cladding due to the high energy of

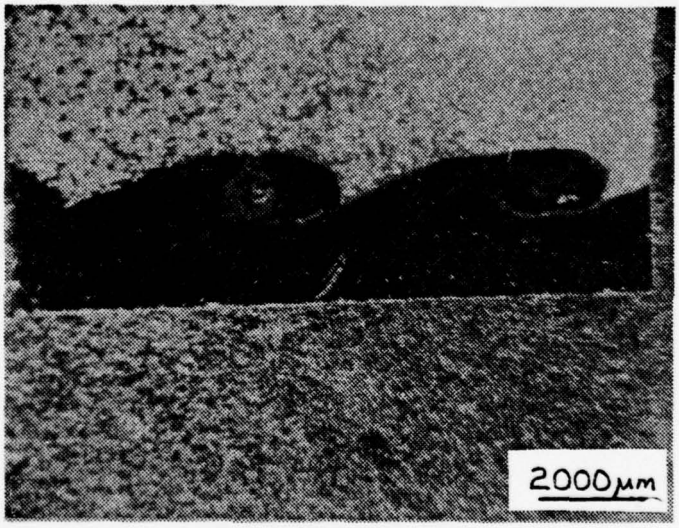

Figure 18. 7x binocular photomicrograph of steel-aluminum bond (aluminum-top, steel-bottom). Sample held in bakelite mount.

collision [26]. Figures 19 and 20 are higher magnification of one of the steel waves. The shape and location of the melt illustrates the fluidity at the interface during forming. Two small voids are also evident. Voids of this size would normally not be noticed in selecting representative samples. The actual samples used had similar profiles but were not as readily discernible because they were not polished.

The standard test samples were finished with #50 grit sandpaper. Figure 21 shows the interface running vertically, with the aluminum on the right. The surface appearance is characteristic of all samples in their unexposed state. Sanding was accomplished from left to right and was intended to be as nearly perpendicular to the overall interface plane as possible. In the center right of the picture, some sanding grooves tend to cover other grooves. This feature becomes more difficult to distinguish farther away from the interface and at higher magnifications. The aluminum is obviously much more deeply grooved than the steel and appears to be somewhat recessed from the level of the steel. Both of these features are quite reasonable, given that 1100 aluminum is a much more malleable metal. Particles of the worked metal and sanding material can be seen at the interface. The surface profile seen may be very distinct; but since the bonded joints are truly three-dimensional, a completely different profile might reasonably exist at a relatively short distance into the metal. Therefore care must be exercised before attributing an apparent undercutting of one bond face surface or another to a corrosion process.

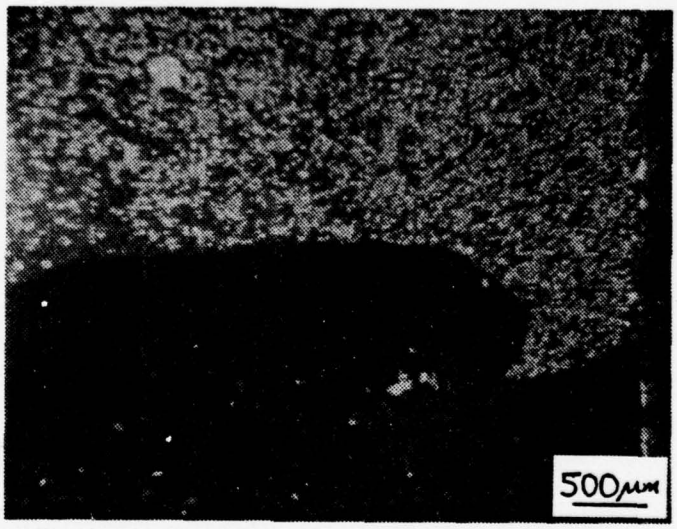

Figure 19. 20x binocular photomicrograph of steel wave with melt (Aluminum over Steel).

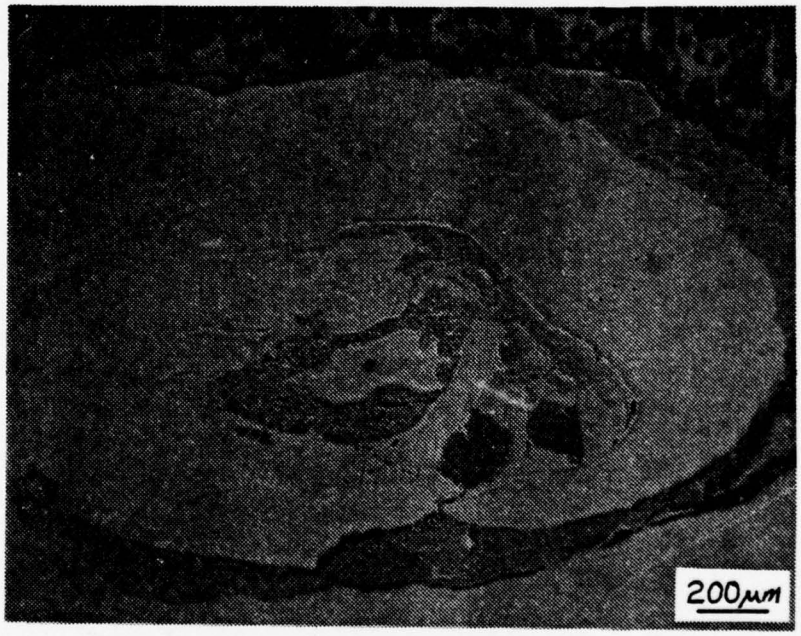

Figure 20. 50x B&L Bench Metallograph photo of steel wave and melt. Dark porous material around the top is aluminum. White material is steel. Gray material is melt.

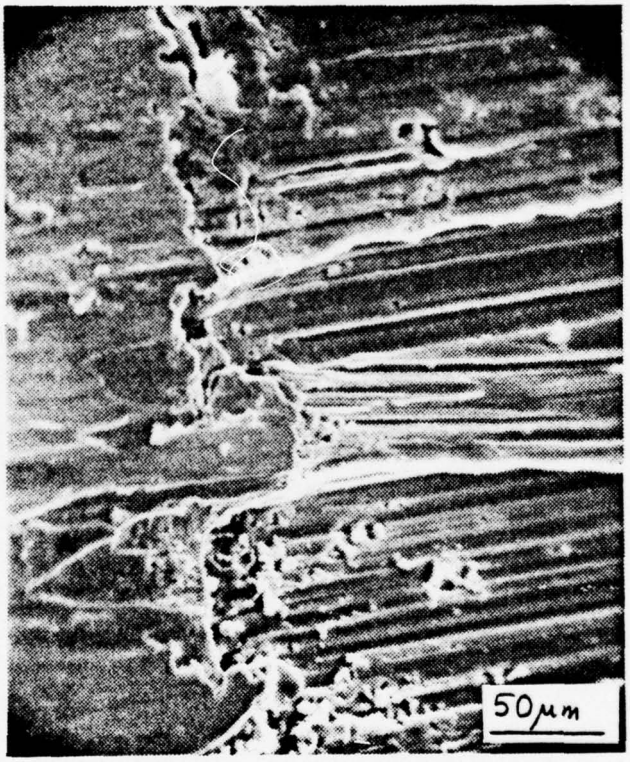

Figure 21. 320x SEM photograph of steel-aluminum interface in the as-sanded condition (Steel←→Al).

Examination of the aluminum side of a sample, Figure 22, shows a very rugged surface contour. Here again, the overlapping of sanding grooves can be seen. The aluminum can generally be distinguished from the steel, in the as-sanded condition (Figure 23) by the degree of roughness of the surface. The steel tends to have a more gently curved appearance with occasional sharp edge, while the aluminum shows deep grooving, many ridges, and a generally jagged surface.

B. SHORT TERM EXPOSURE

All samples were placed in the testing tank at the initiation of the experiment. At predetermined time intervals one sample from each wheel was removed, rinsed, and mounted. After mounting, each sample would be viewed with the binocular microscope to observe gross surface effects, and then with the SEM to examine micro-activities. Comparison photographs of similar areas on each sample were taken, at corresponding magnifications, in an attempt to correlate the number of spray exposures to the amount of corrosion. The first two samples were removed after 30 minutes. This corresponded to six sprayings of one sample and 15 of the other. At the interface region on both samples, a visible band has developed on the aluminum side, Figures 24 and 25. The aluminum in this band appeared to be somewhat less jagged but still had the same general grooving detail as the aluminum farther away. It is believed that this effect is due to the aluminum immediately adjacent to the bond behaving anodically with respect

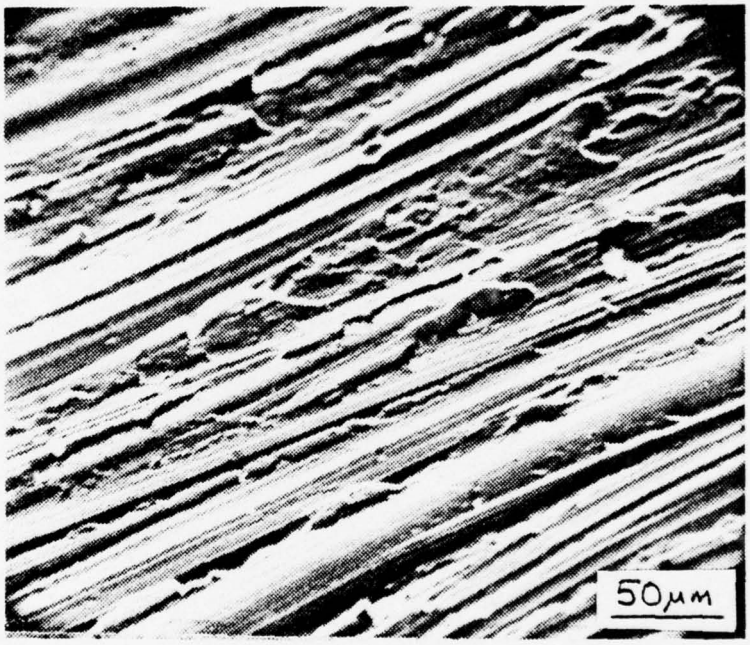

Figure 22. 320X SEM photograph of unexposed aluminum half of typical sample in an as-sanded condition.

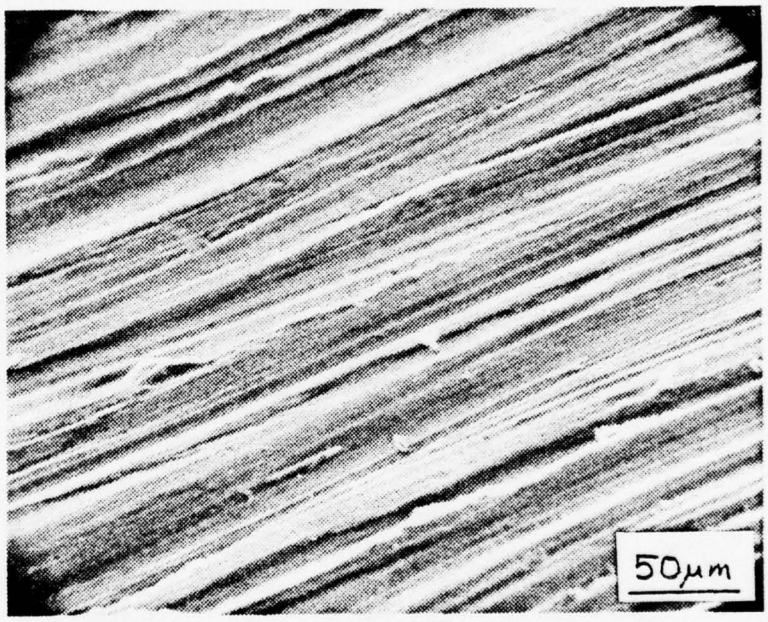

Figure 23. 320X SEM photograph of unexposed steel of a typical sample in an as-sanded condition.

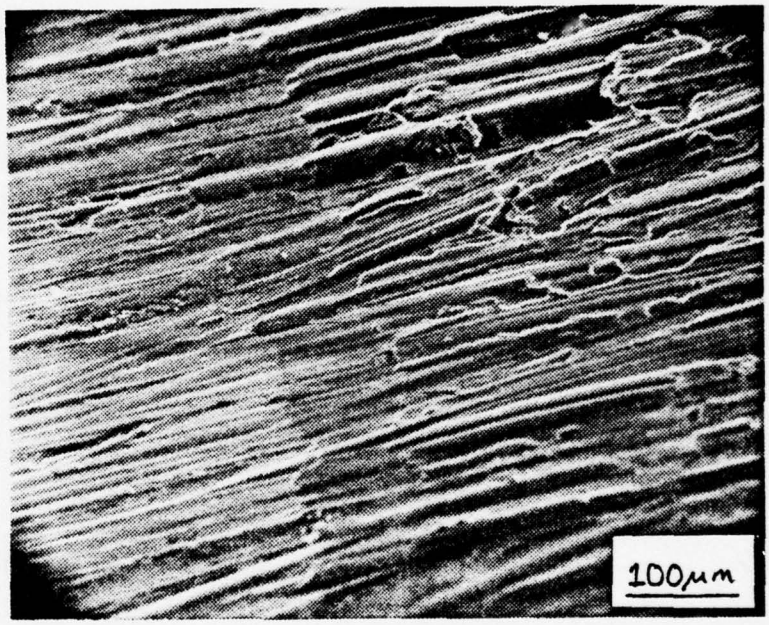

Figure 24. 160x SEM picture of the interface region showing corrosion band after 30-minute exposure and six sprayings (Steel←→Al).

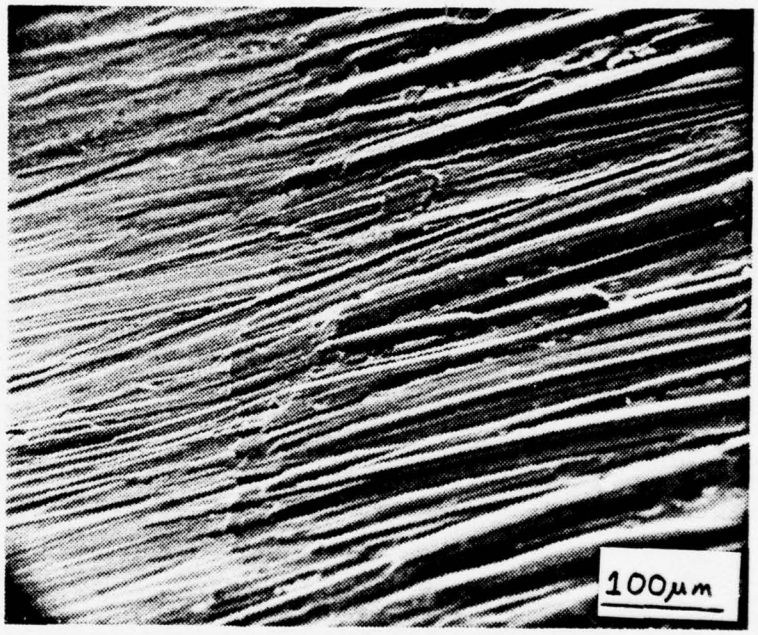

Figure 25. 170x SEM picture of the interface region showing corrosion band after 30-minute exposure and 15 sprayings (Steel←→Al).

to the steel and experiencing accelerated deterioration. The corrosion attacked the sharpest features most severely but removed metal generally throughout the bond. Thus the ruggedness of the surface appears decreased. As the distance from the interface increased, the galvanic couple had less affect and the concentrated deterioration decreased, while at the interface the line of demarcation sharpened. Although the two samples had contour differences, there did not appear to be any significant differences at the bond that were attributable to variances in the number of spray exposures. Figure 26 is a picture of the bond at a higher magnification. The right side of the corrosion belt is outside of the view of the picture. Localized anodic dissolution pitting appears in the aluminum next to the bond, about 3 cm from the top of the picture. In this photograph an almost indiscernible haze film extends for a relatively short distance on both sides of the interface. For this exposure time, neither specimen showed significant differences from the unexposed samples in the area on the aluminum further from the bond, Figures 27 and 28. On the steel side of the samples, the specimen with the fewest sprayings appeared similar to the unsprayed sample at 340x, Figure 29, while the more frequently sprayed sample showed the first signs of rust deposit formation, Figure 30. No evidence of general film or scale formation was observed on the steel, even when examined up to 5000x.

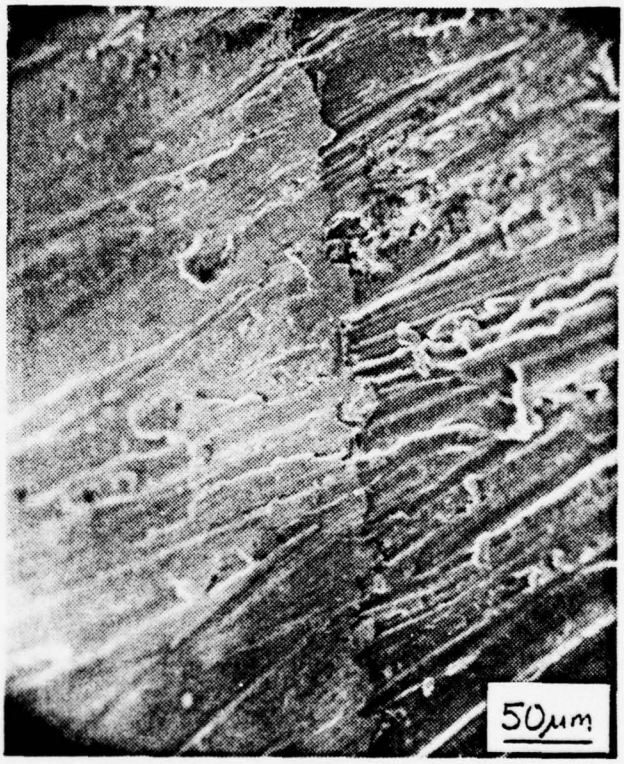

Figure 26. 250x SEM picture of bond area and corrosion belt showing localized anodic dissolution after 30-minute exposure and 15 sprayings (Steel←→Al).

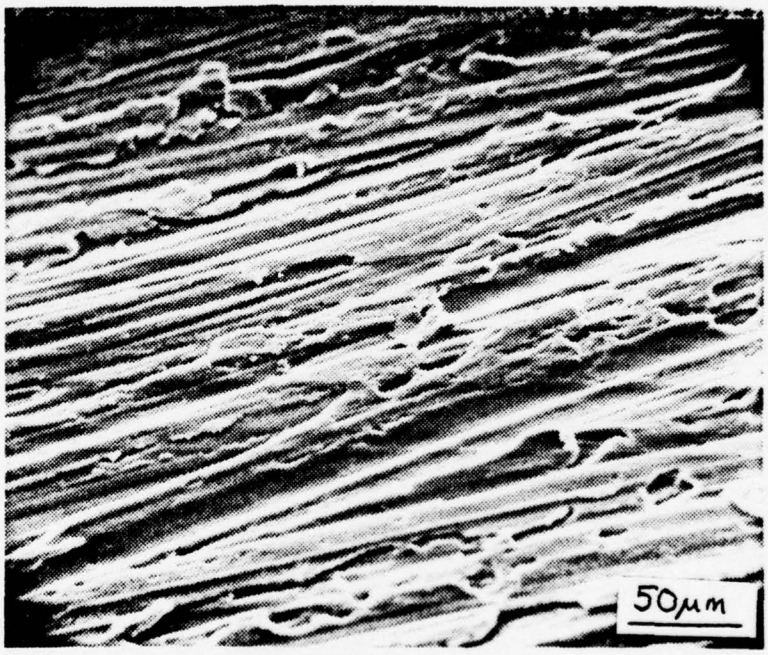

Figure 27. 320x SEM photograph of aluminum away from interface after 30-minute exposure and 15 sprayings.

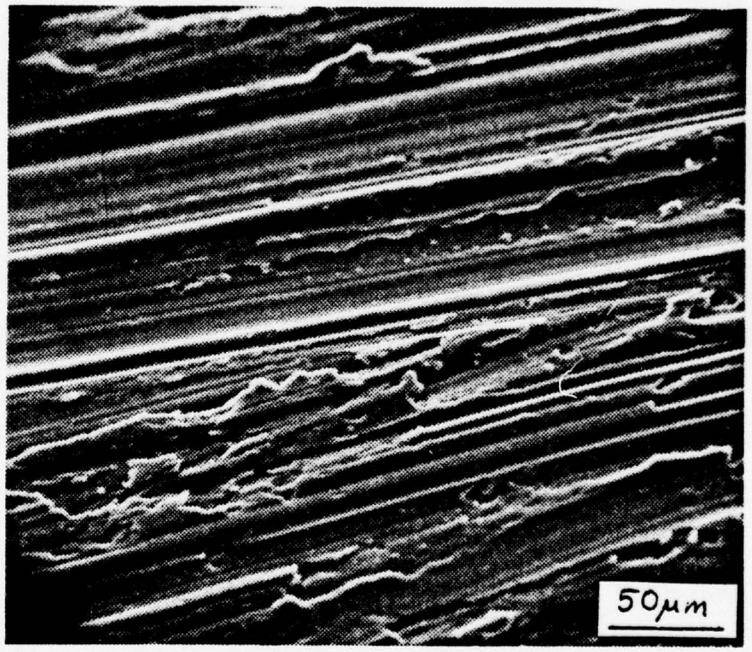

Figure 28. 320x SEM photograph of aluminum away from interface after 30-minute exposure and six sprayings.

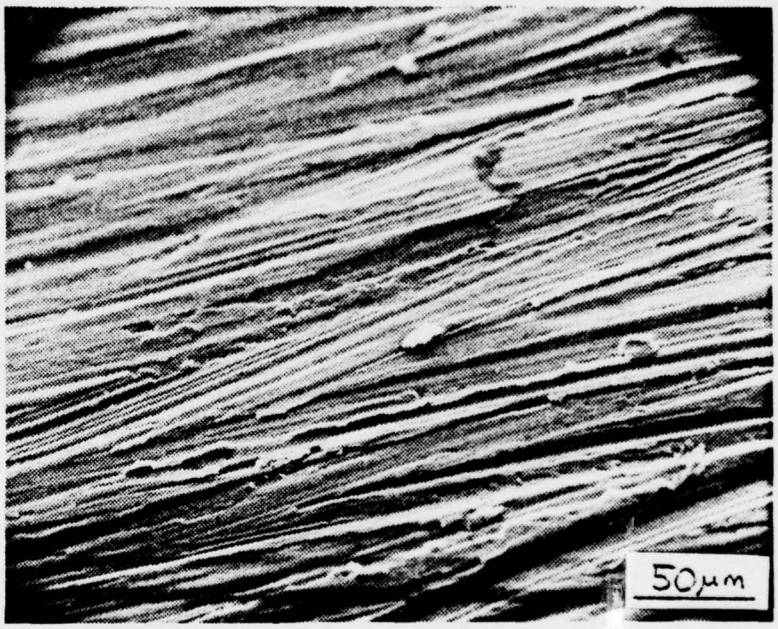

Figure 29. 340x SEM picture of steel away from bond after 30-minute exposure and six sprayings.

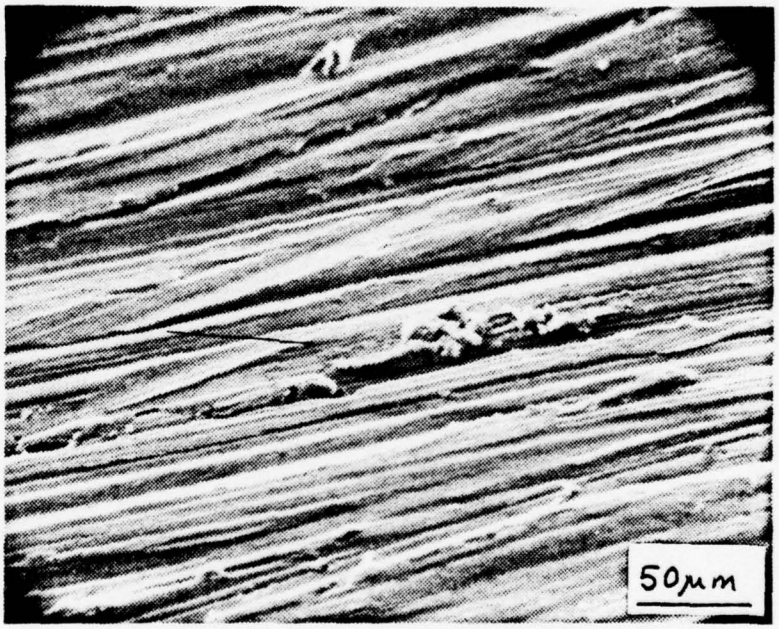

Figure 30. 320x SEM picture of steel away from bond showing initiation of rust deposits after 30-minute exposure and 15 sprayings.

The next pair of samples were removed after one hour, with 12 and 30 sprayings respectively. Again a corrosion belt was visible near the interface, Figure 31, but it seemed to disappear in some areas. The aluminum within this bond appeared smoothed, with distinct ridges separating it from both the steel and the rest of the aluminum. Small clumps of pebble-shaped rust deposits could be seen near the interface on the sample that received more spray. When viewed at a lower magnification the steel side of the interface showed a build-up of an almost transparent film with a few tiny specks of rust popping through. The film build-up was much thicker in places, Figure 32, and could be seen as a white trail originating at the interface. This was probably due to precipitation of the oxide compounds formed at the interface but carried over to the steel by gravitational flow of the solution. Enlarged views of these areas show a build up of snowflake-like particles beginning immediately at the interface on the steel, but a complete absence of these particles on the aluminum, Figures 33 and 34. In Figure 35, the interface was enlarged to 1300x. At this magnification a distinct area of micro-anodic activity can be seen. Slightly to the top left of center in this picture there is a relatively deep valley in the aluminum adjacent to the bond face. The white trail previously described was located near this pit. As one might expect, areas of high interface activity generally were adjacent to heavy deposit trails. Again, for this

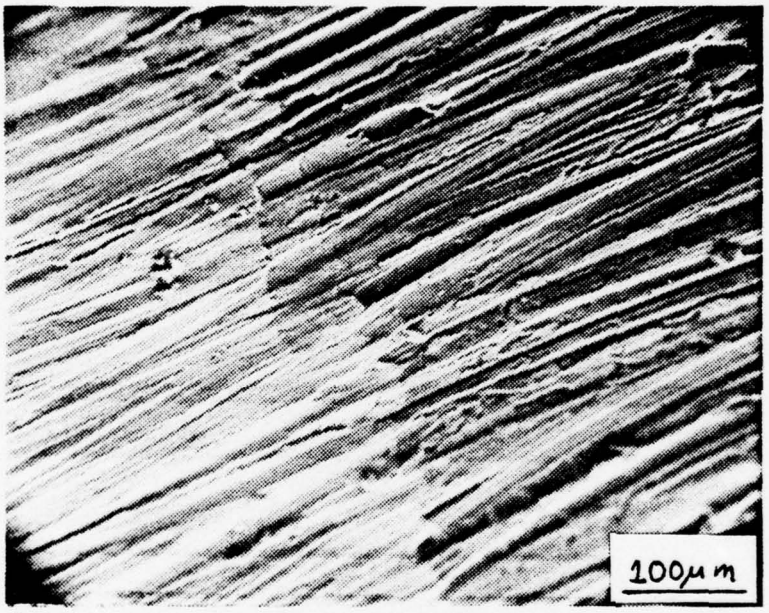

Figure 31. 175x SEM photograph of the interface illustrating the corrosion band and small clumps of rust after one-hour exposure and 30 sprayings (Steel←→Al).

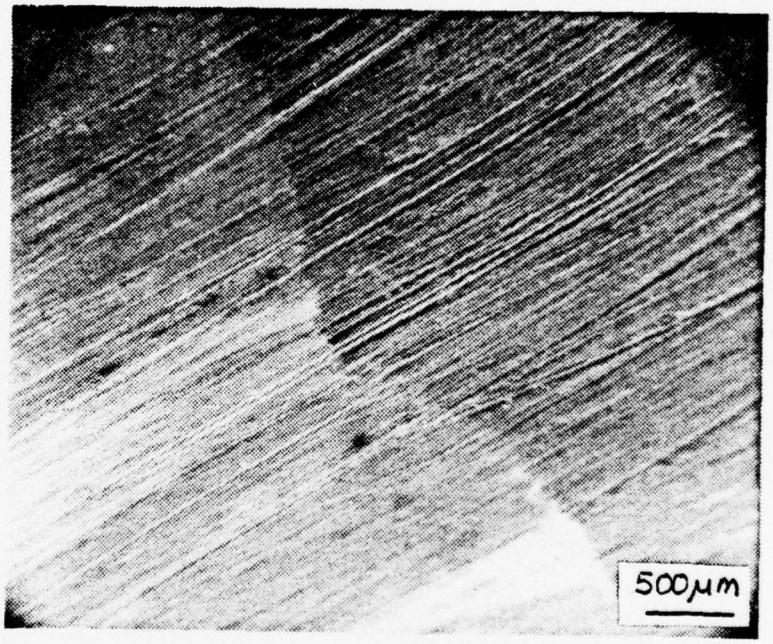

Figure 32. 25x SEM photograph showing the bond interface with trail of white deposits on the steel after one-hour exposure and 12 sprayings (Steel←→Al).

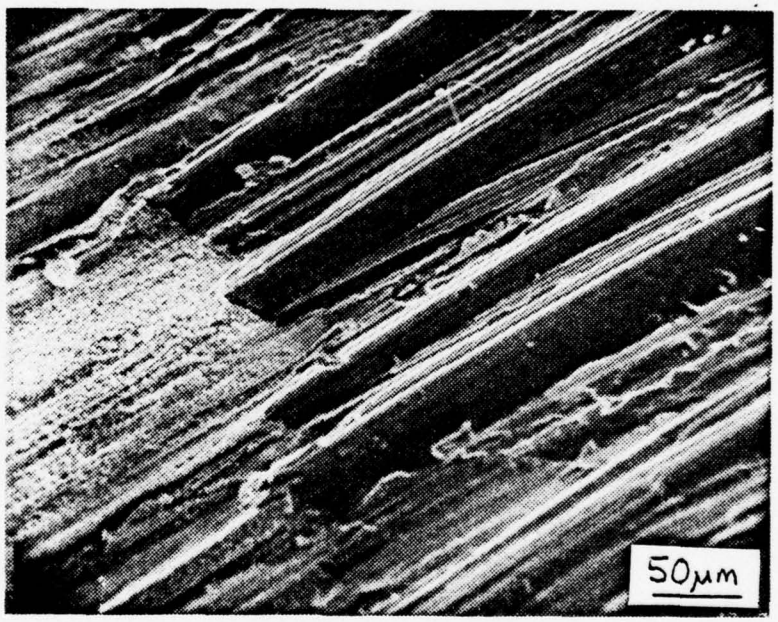

Figure 33. 250x SEM picture of interface showing small deposits on steel after one-hour exposure and 12 sprayings (Steel←→Al).

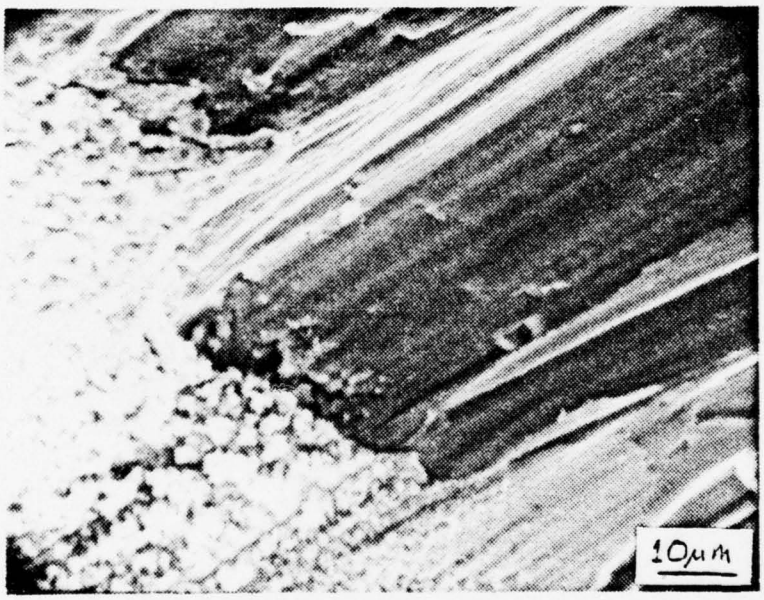

Figure 34. 1100x SEM photograph of interface showing snowflake-like build-up on steel with no build-up on the aluminum. Sample had one-hour exposure and 12 sprayings (Steel←→Al).

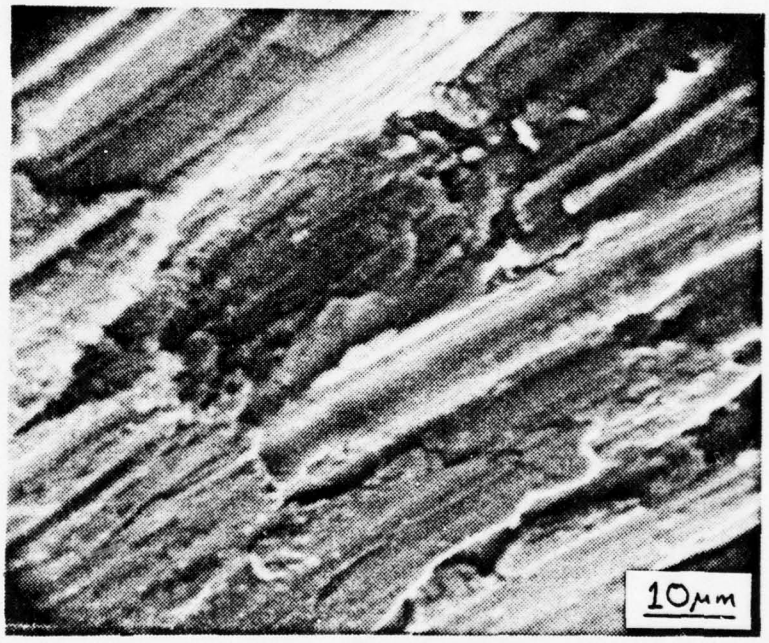

Figure 35. 1300x SEM picture of interface after one-hour exposure and 12 sprayings shows microanodic valley.

exposure time, very little change from the unexposed samples was observed on the steel away from the bond. It did have small rust deposits and the previously mentioned trails, but no general coating was observed up to 5000x. Trace scaling did begin to appear on both aluminum samples at about 2000x. Even though this scaling was small, the jagged edges and ridges on the aluminum began to appear to be covered with a hazy film, Figures 36 and 37.

During examination of surface particles of alumina (Al_2O_3) and iron oxide (Fe_2O_3), the PGT-1000 was often used. By using high magnification and isolating the beam on one of these particles, the energy-dispersed x-ray spectrum from the base metal underneath them could be nearly eliminated. This analysis did not, of course, unambiguously determine the compounds that were deposited, but the base metal (Al or Fe) from which they derived could be determined. For example, in the case of the deposits previously seen in Figures 33 and 34, even though the white trail was physically located on the steel, the x-ray spectrum indicated an aluminum-based compound, and it could be surmised that the deposits were most likely alumina, Al_2O_3. The identity of the previously-mentioned small pebbly clumps as iron oxide, rust, was ascertained in a similar fashion. Unlike the alumina deposits, the iron oxide particles were located on a base metal that would give a similar readout on the x-ray analyzer. Therefore the size, shape and location of the particles were correlated with those of particles viewed on the same sample under the binocular

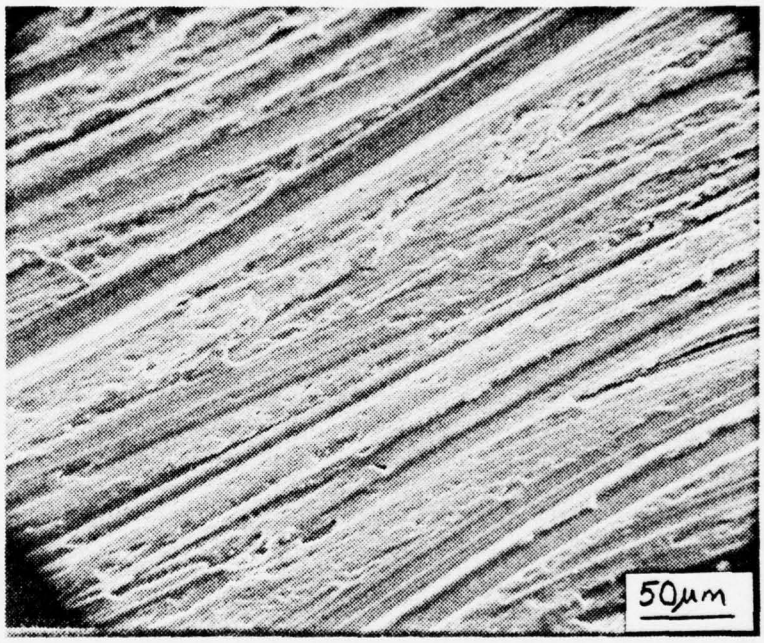

Figure 36. 260x SEM photograph of aluminum taken after one-hour exposure and 12 sprayings. It shows slightly hazed tone of fringes.

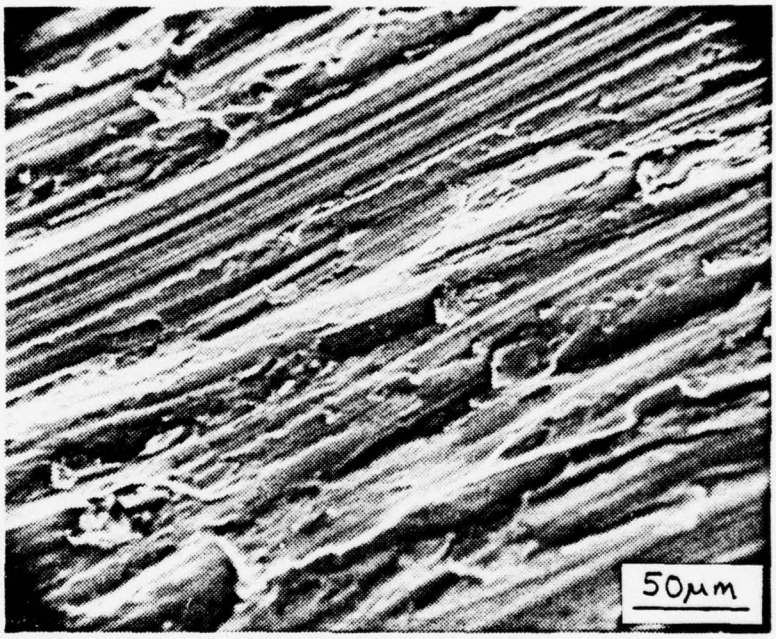

Figure 37. 320x SEM picture of aluminum taken after a one-hour exposure and 30 sprayings. Shows hazy tone of fringes.

microscope, where the deposits were seen to have a typical iron oxide rust color.

Two more samples were removed after two hours total exposure. For all practical purposes these samples had nearly identical corrosion development. This proved to be the case for subsequent samples also;and,therefore,distinctions will no longer be made between one sample and another on the basis of frequency of spraying. Samples will be identified only by the duration of their exposure. One sample of each lot will be described,and only the unusual features of the other sample will be noted.

The two-hour samples still showed some signs of a belt corrosion zone, Figure 38, but the belt did not extend over as much of the length of the interface as it previously did. Beyond this band on either side, definite signs of corrosion and deposit build-up were evident. This was especially true on the aluminum side. Heavy deterioration of the sanding fringes and most rugged regions could be seen. Moving along the interface line, it became evident that sections of the bond area had become almost completely covered with corrosion products. In Figure 39 some grooves in the aluminum can be seen to be partially covered near the interface while others are completely obscured. In the upper part of the picture the surface shows a hazy contrast, similar to the light cloud cover often seen from airplane windows. While the surface markings can still be observed through this hazy film formation, it is apparent that it is

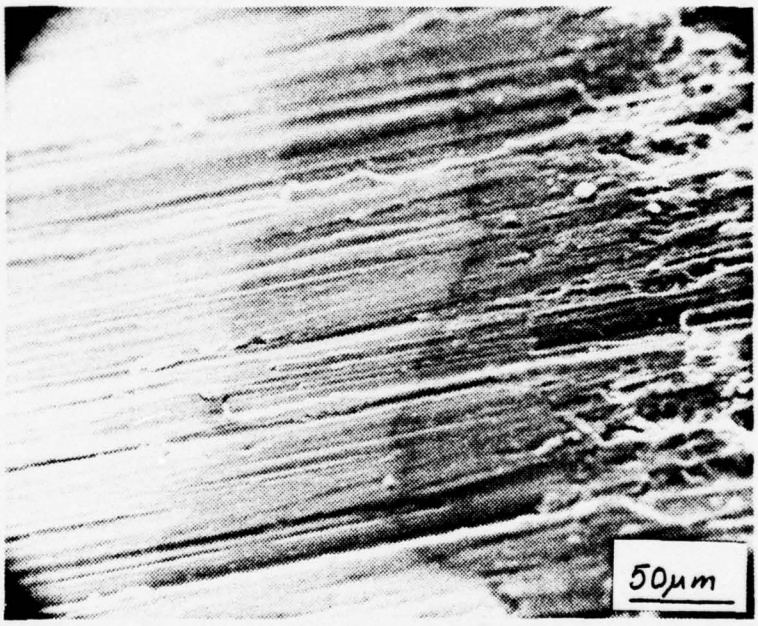

Figure 38. 290x SEM photograph of interface after two-hour exposure showing belt zone and adjacent films (Steel←→Al).

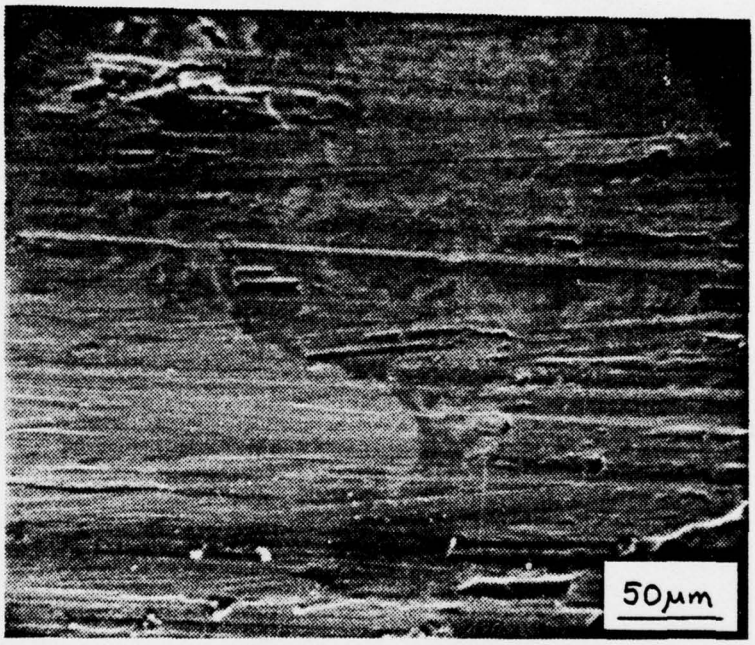

Figure 39. 300x SEM picture of interface after two-hour exposure showing hazy film coverage over most areas (Steel←→Al).

increasing in thickness and is nearly opaque in places. A similar process, though somewhat less dramatic, was taking place generally over all of the aluminum surface. The aluminum shown in Figure 40 still has definite grooving marks, but much of the contour runs across these marks, thus indicating growth subsequent to sanding. The overall surface appearance is hazy, and has fewer recognizable features. The same general hazy overcast appearance is present on the steel. Along with this is a marked increase in the rusting activity. Macroscopically, after two hours, rusting was visible to the naked eye. Figures 41, 42 and 43, in order of increasing magnification, show a typical area of steel with nodular groupings of rust. The nodules appear to be closely grouped spherical pebbles at low magnification. The same characteristic shape is observed when very small groupings are viewed at high magnification, Figure 42. The growth seems to locate close to surface irregularities on the steel. As the spheres grow in size some tend to split open like clam shells. At lower magnification, the opened ones appear to have dark spots in the middle. Figure 43 shows some larger particles at higher magnification.

At the end of six hours of exposure the interface area had become heavily covered with corrosion product. The aluminum grooves could still be seen in places, but for the most part the bond interface had actually been obscured by the deposit of alumina. Pinpointing the actual interface was nearly impossible because of the buildup, but the growth

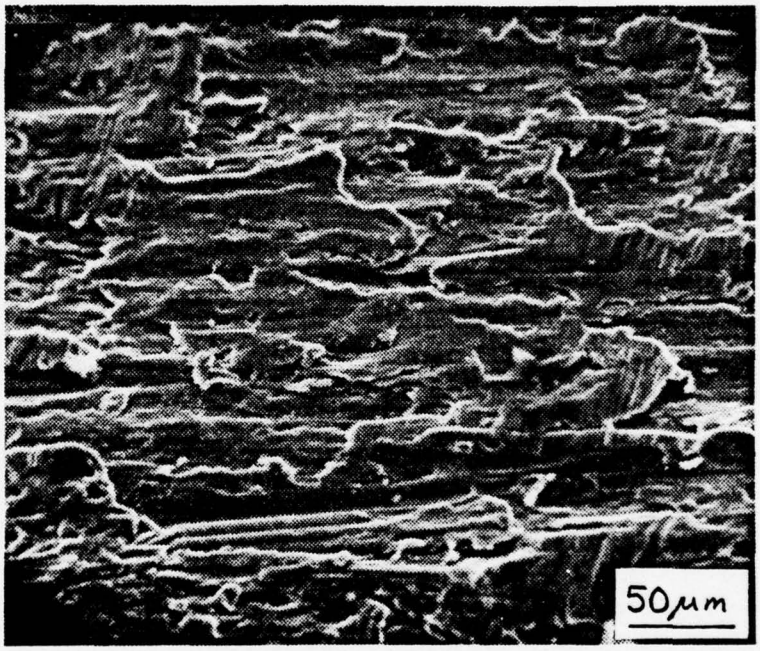

Figure 40. 300x SEM photograph of aluminum after two-hour exposure. It shows general surface deterioration and loss of features.

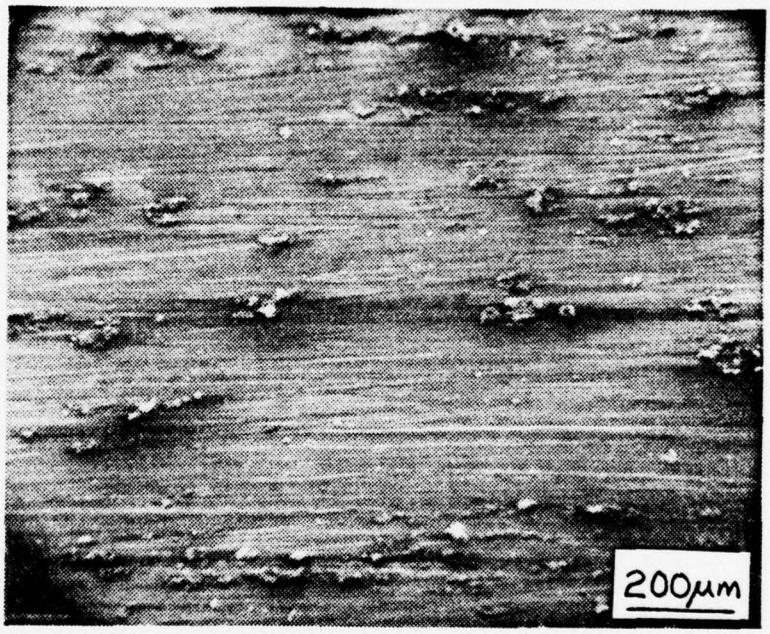

Figure 41. 75x SEM picture of rust nodules formed over layer of alumina film on steel after two-hour exposure.

Figure 42. 700x SEM picture of beginning of rusting at surface deformity on steel after two-hour exposure.

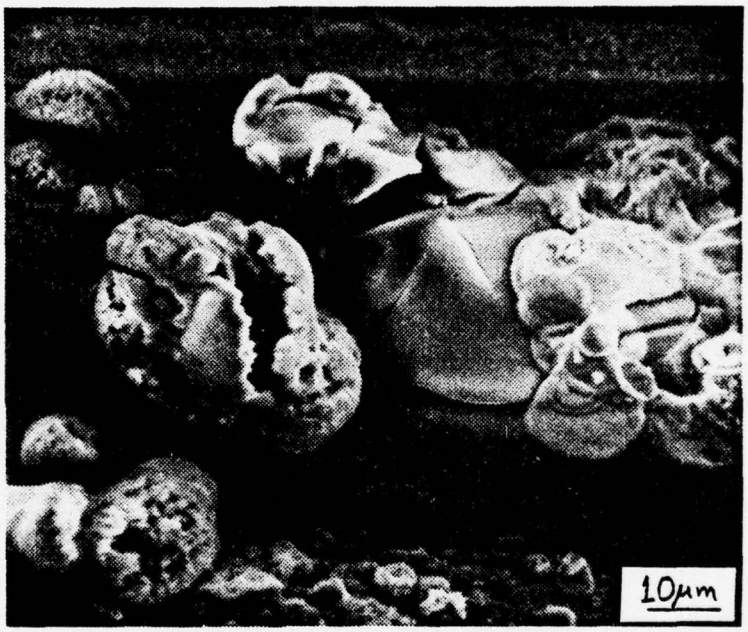

Figure 43. 1050x SEM picture of rust particles on steel surface after two-hour exposure.

exhibited some of the contour of the surface beneath it, so that examinations in the proximity of the interface were possible. Figure 44 shows the surface scale in and around the bond. Higher magnification views of this rough area tended to yield very little information. A picture of a less rugged segment of the bond area is shown at 1350x in Figure 45. The larger scale formations on the left conform closely to those previously seen on the steel side of the bonds. The clear break in levels seems to indicate that the intermediate formation is over the aluminum. This is indicated to be the case by the appearance of the aluminum grooves at the top right. The alumina seems to be settling out and gradually filling in the corrosion band. The intermediate level can be seen to have a checked appearance similar to the steel, but with the scales much smaller in size. This same type of formation seems to be covering the aluminum in general, as seen in Figure 46. The individual scales are nearly invisible at this magnification but when the picture is enlarged they become very prominent. The texture of the alumina film at 2800x looks quite similar to that of a head of cauliflower, Figure 47. Not surprisingly, a similar morphology exists on the open areas between the rust pebbles on the steel, Figure 48. This indicates that eventually the alumina tends to precipitate out on the entire sample.

After 12 hours of exposure the interface was virtually covered with alumina deposit. The size of the scales on the steel near the interface was generally larger but those on

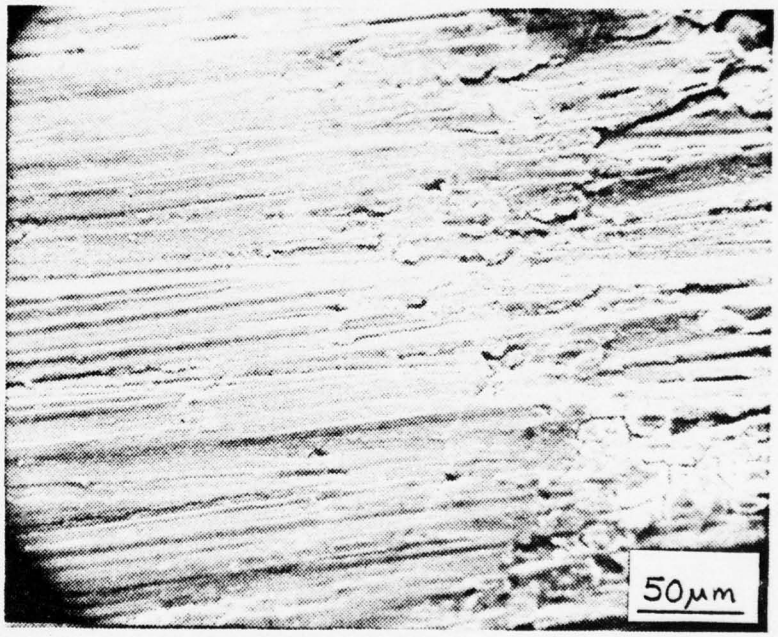

Figure 44. 305x SEM picture of bond area after six-hour exposure shows heavy corrosion obscuring the interface (Steel←→Al).

AD-A032 365 NAVAL POSTGRADUATE SCHOOL MONTEREY CALIF F/G 11/6
MICROSCOPIC INVESTIGATION OF INTERFACE CORROSION OF STEEL-ALUMI--ETC(U)
SEP 76 M R KEELEAN

UNCLASSIFIED NL

2 OF 2
AD
A032365

END
DATE
FILMED
1-77

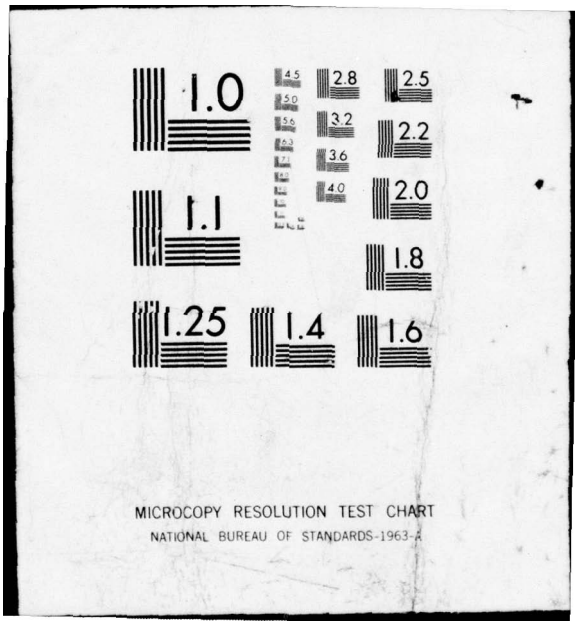
1.0
1.1
1.25
1.4
1.6
1.8
2.0
2.2
2.5
2.8
3.2
3.6
4.0
4.5
5.0
5.6
MICROCOPY RESOLUTION TEST CHART
NATIONAL BUREAU OF STANDARDS-1963-A

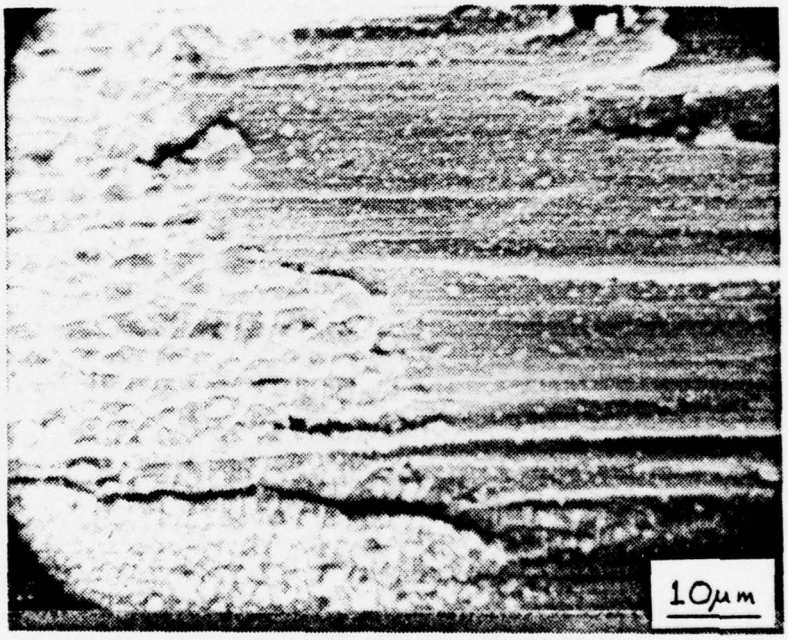

Figure 45. 1350x SEM photograph of bond area after six-hour exposure showing general scale growth on the steel and a base scale growth starting to cover the aluminum (Steel←→Al).

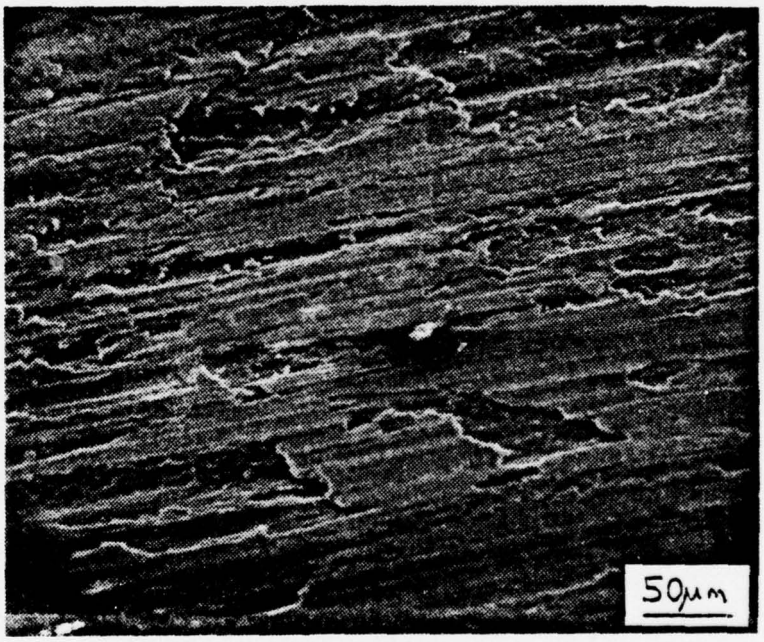

Figure 46. 250x SEM picture of the surface film over aluminum after six-hour exposure.

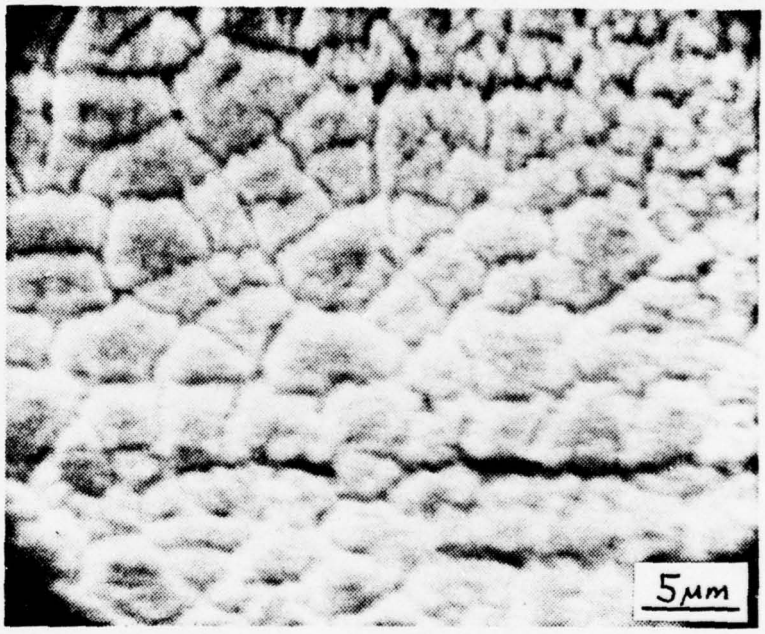

Figure 47. 2800x SEM picture of alumina scale on aluminum after six-hour exposure.

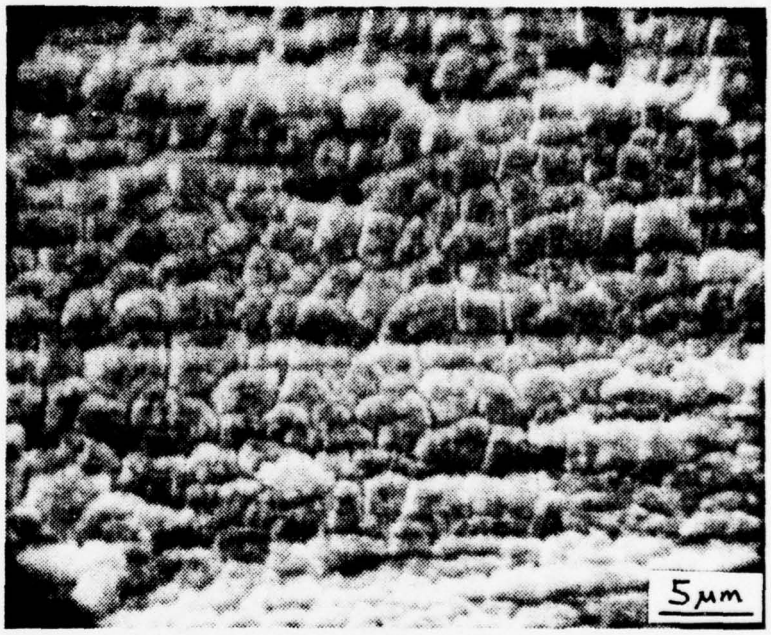

Figure 48. 2700x SEM picture of alumina precipitated onto the steel after six-hour exposure.

the aluminum were beginning to grow. Surface features, though still generally recognizable, were becoming far less distinct. Figures 49 and 50 show the bond areas at different magnifications. The scale formations of alumina were still not apparent at 240x after 12 hours even though the surface appears to be covered, Figure 51. At 2400x the by now familiar dried-and-checked-paint appearance again can be seen, Figure 52. On the steel side of the samples, the alumina film appears to have formed a nearly continuous coating over the entire surface, Figure 53, with interspersed appendages of iron oxide. Figures 54, 55 and 56 show that the alumina film actually exists right up to and perhaps underneath the rust particles. The rust may have formed prior to the alumina film, or broken through the cracks after the film had formed.

Subsequent samples were removed at the one- and two-day points to the experiment. Examination of these specimens indicated that the coverage of the alumina film was practically complete. The size of the scales continued to increase, and on the one-day samples was visible down to about 300x at the interface, and down to about 160x on the aluminum farther away, Figures 57, 58 and 59. Figure 60 is a low magnification picture of the steel side of the sample after two-day exposure. Clearly, the rusting has greatly increased even though the alumina had formed a film on the steel. Figure 61 shows a ferric oxide growth initiating through the alumina film.

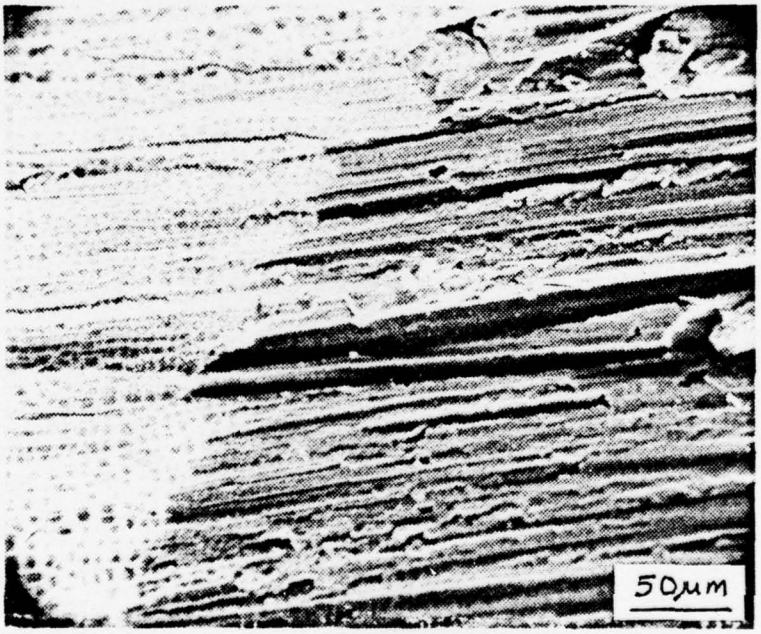

Figure 49. 280x SEM picture of the bond interface area after 12-hour exposure (Steel←→Al).

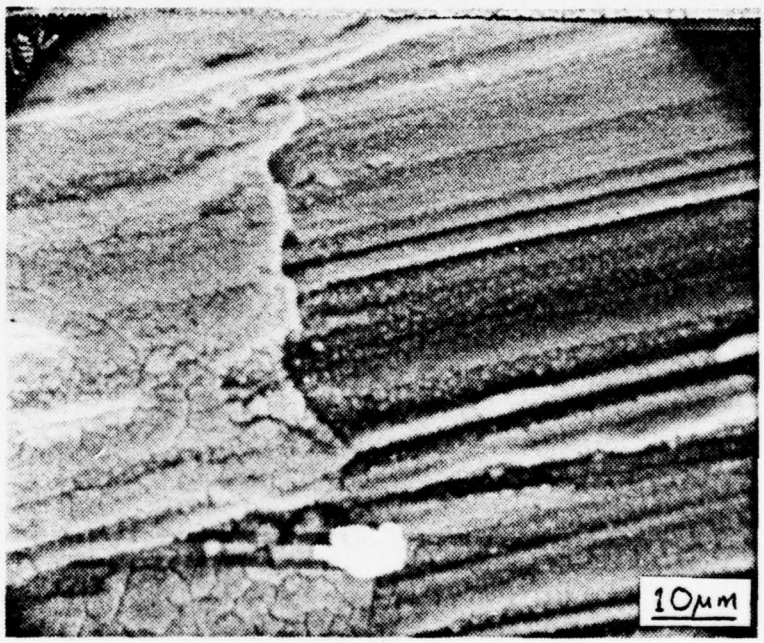

Figure 50. 1200x SEM picture of bond area after 12-hour exposure (Steel←→Al).

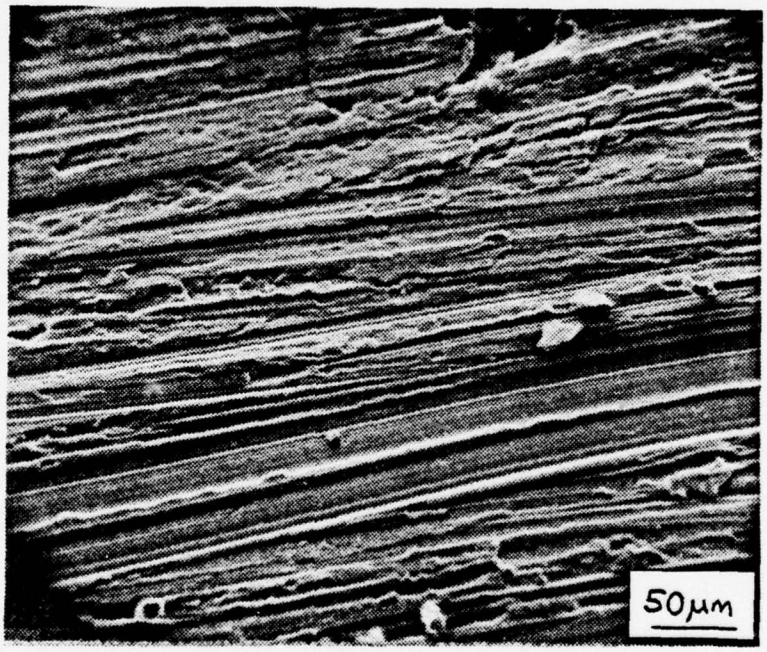

Figure 51. 240x SEM picture of aluminum after 12-hour exposure.

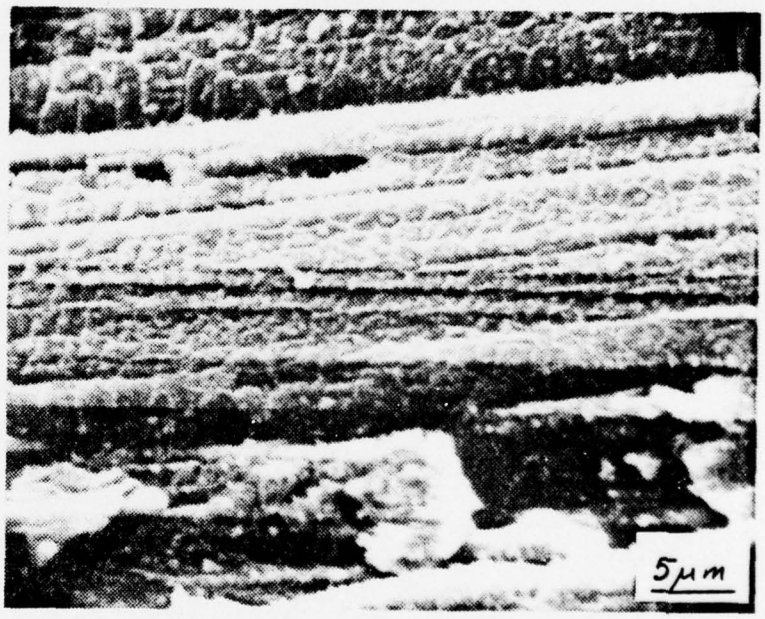

Figure 52. 2400x SEM picture of aluminum surface film after 12-hour exposure.

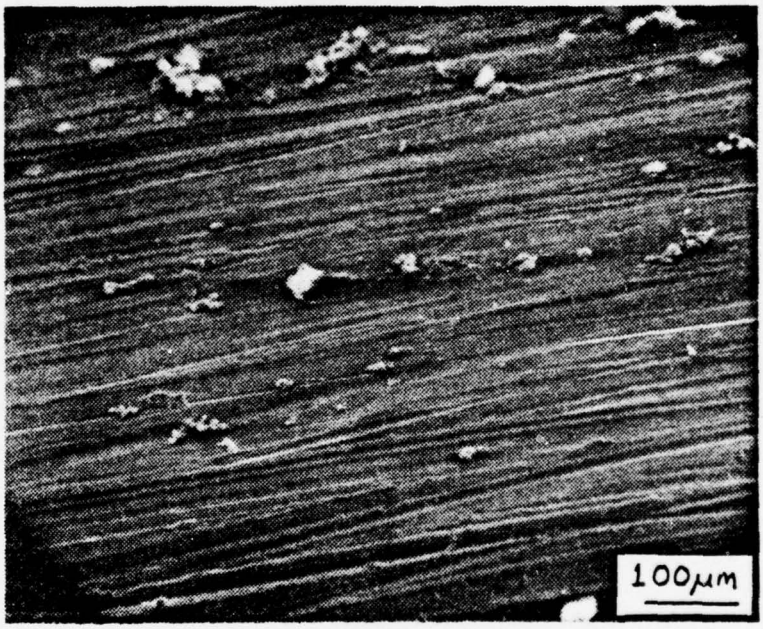

Figure 53. 130x SEM picture of steel with coating of alumina and rust nodules after 12-hour exposure.

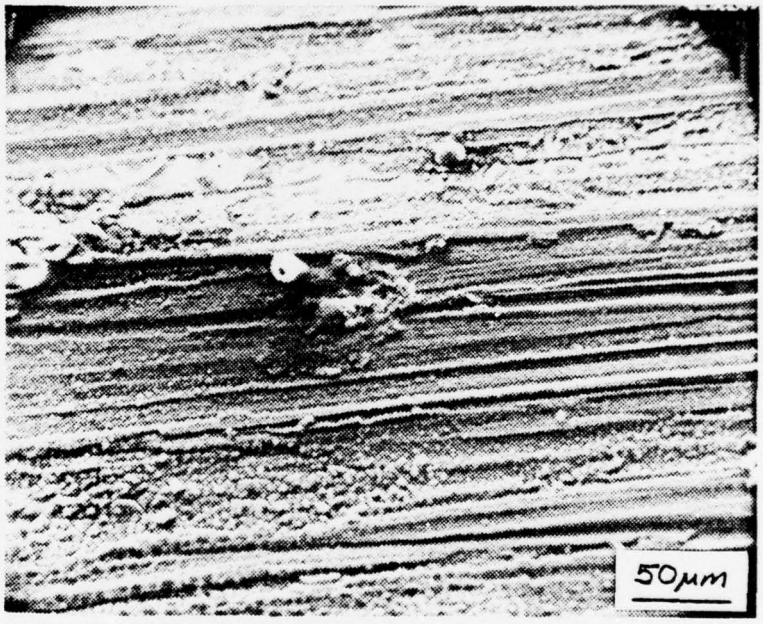

Figure 54. 280x SEM picture showing iron oxide growth in alumina coating on steel after 12-hour exposure.

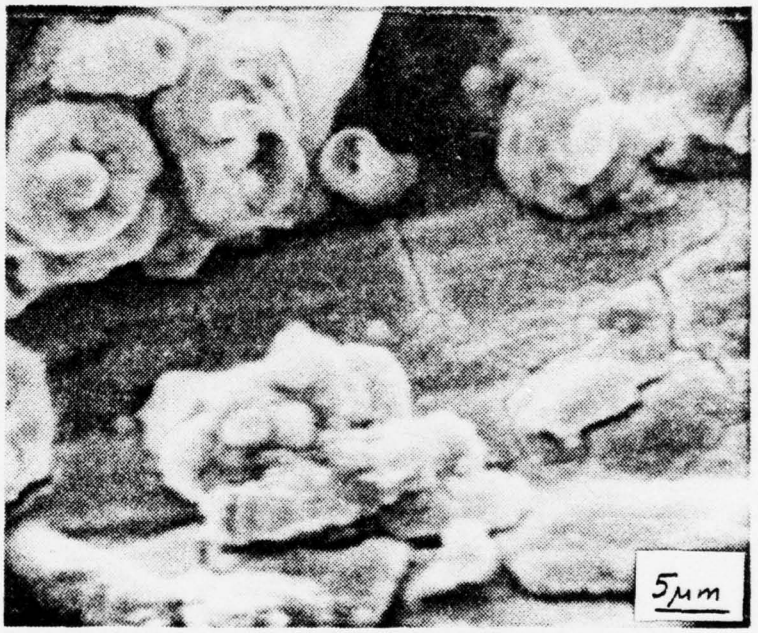

Figure 55. 2050x SEM picture showing iron oxide growth through film of alumina on steel after 12-hour exposure.

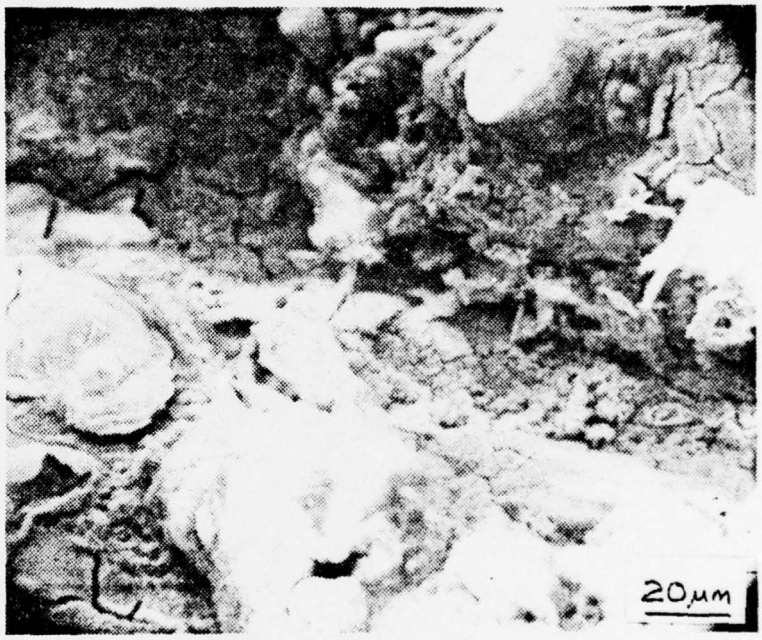

Figure 56. 600x SEM photograph of rust and alumina formation on steel after 12-hour exposure.

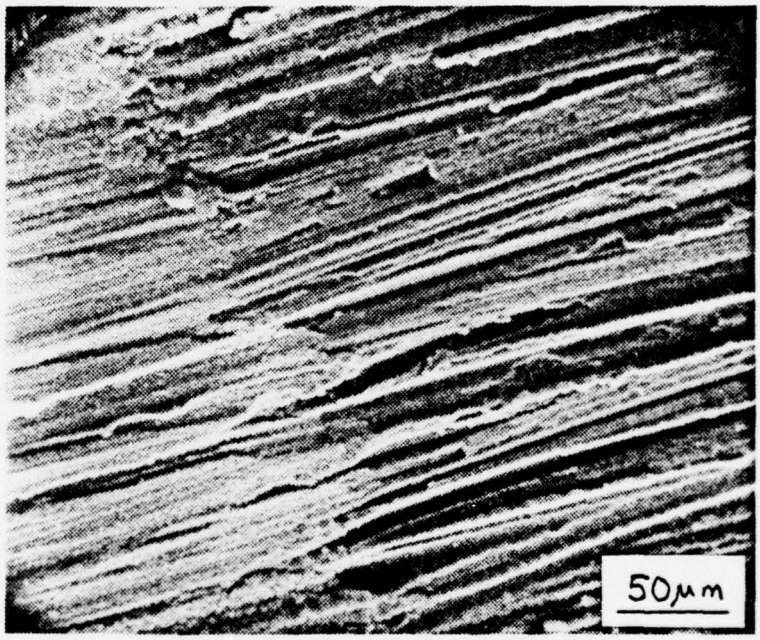

Figure 57. 320x SEM picture of bond interface area after one-day exposure (Steel←→Al).

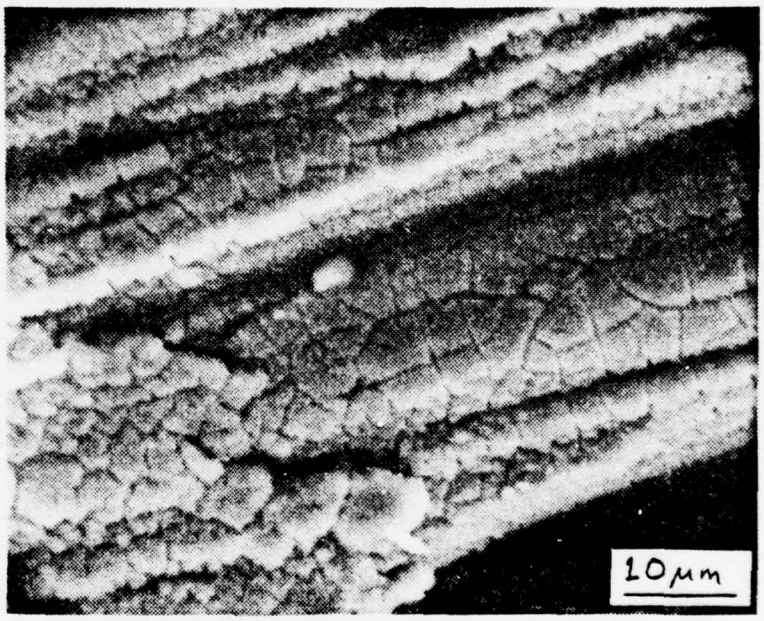

Figure 58. 1600x SEM picture of bond area showing complete coverage by alumina after one-day exposure (Steel←→Al).

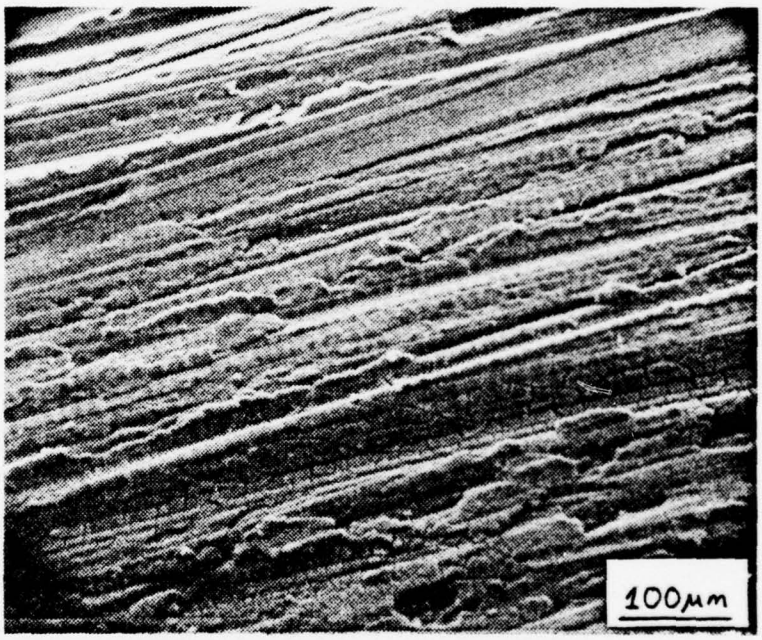

Figure 59. 160x SEM picture of alumina on aluminum surface after one-day exposure.

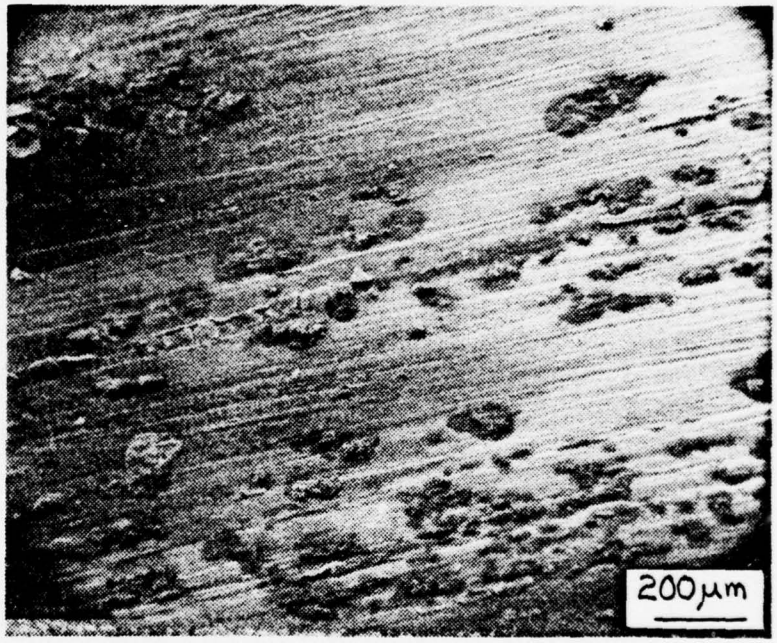

Figure 60. 65x SEM picture of rusting on steel half of sample after two-day exposure.

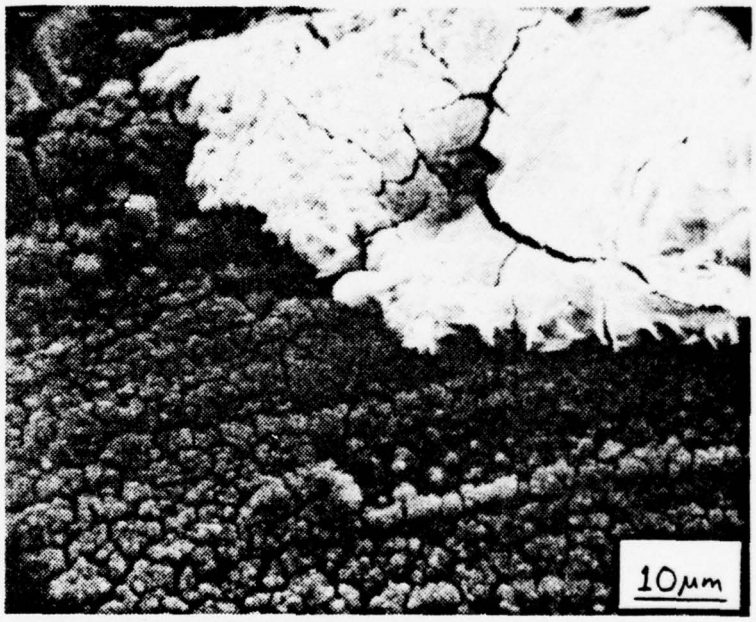

Figure 61. 1300x SEM picture of rust exploding through layer of alumina scale after two-day exposure.

C. LONG TERM EXPOSURE

Once passivation between one and two days became evident, samples were removed weekly up to nine weeks. During the first two weeks, examination of the samples indicated that rusting on the steel continued, as expected, and that corrosion at a few interface locations persisted in spite of the passivating alumina film. At first this corrosion at the interface was attributed to sample imperfections or abnormalities. Upon comparative examination of second- and third-week specimens, it began to appear that the samples not only had pockets of continued corrosion but that these pockets located themselves in relatively standard positions with respect to the wave line. Therefore all samples exposed from three to nine weeks were examined as a group to better categorize the commonalities among them. Contrary to what was anticipated, the corrosion and formations observed did not appear to be directly related to the exposure times. That is, while samples at seven weeks exposure had more corrosion than those at three weeks exposure, the samples at four and five weeks exposure had more corrosion than some exposed longer. The location of the corrosion on each sample was common, while the extent of corrosion seemed to differ from specimen to specimen. Therefore for this discussion, the exposure durations will be mentioned briefly to identify the specimens, while the major emphasis will be on describing features of commonality among the group.

Figure 62 is a low magnification picture of a five-week specimen. In this picture, the waves formed during bonding

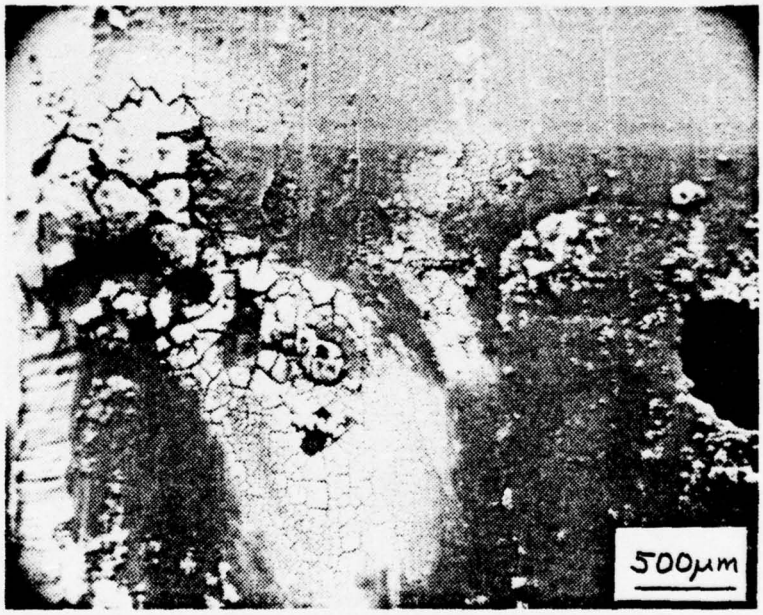

Figure 62. 28x SEM picture of bond zone on five-week exposure specimen showing scaly corrosion product and void (Al over Steel).

proceed from right to left. The large scaly white area typifies one form of continued corrosion appearing on all of the long term samples. Using the identifiable features of the interface in the picture and the knowledge of the general shape of the steel waves as a guide, this corrosion formation appears to be located on the back of one wave near the front of a prior wave. While the sample surface in this area is concealed, it appears that the source of the formation is near or at the bond interface. The dark hole in the center of this white formation is shown enlarged in Figure 63. The previously discussed hydrated alumina scaling is obvious through the hole. The white corrosion product apparently has deposited over this initial film and formed larger scales. The larger scales show a pebbly contour similar to the underlying film. Figure 64 is a picture of the same sample, taken to the right of Figure 62; the void shown is the same one. This void coincides with the vortex of the steel wave. Obvious clusters of iron oxide particles have formed on the wave and partially outline its crest and forward trunk. There was a complete lack of further corrosion, other than rust, around the void in this sample, and this was generally the case for all samples. Still further right of the void in this sample, Figure 65, another mushrooming corrosion growth can be seen. Also, the wave crest and trailing side can be distinguished here, starting about 500 μm above the void and proceeding right, to the corrosion growth. In this trailing-edge area, the passivation appears to have

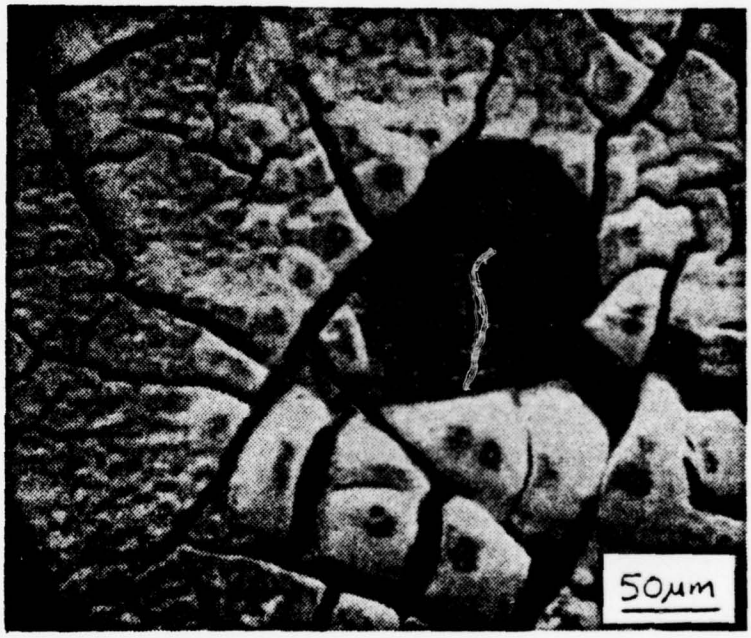

Figure 63. 280x SEM picture of alumina layer beneath second corrosion product film on five-week exposure sample (Steel surface).

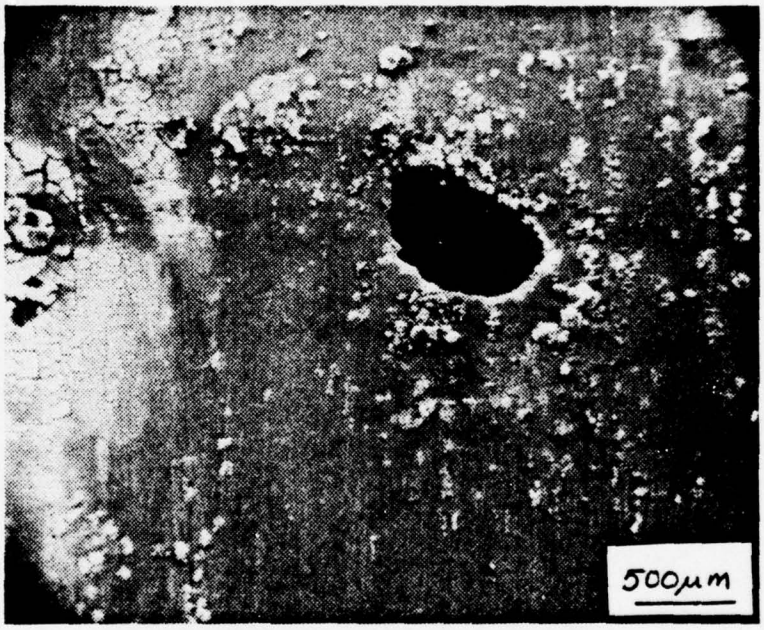

Figure 64. 28x SEM photograph of bond zone on five-week exposure sample showing void and wave outline (Al over Steel).

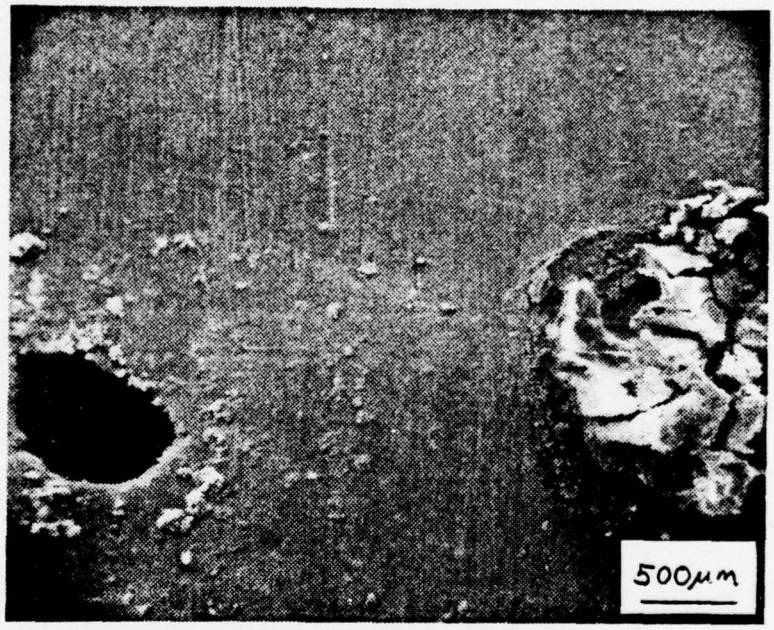

Figure 65. 28x SEM picture of bond zone on five-week exposure sample with void, wave outline, and mushroom-shaped formation (Al over Steel).

taken place as described in the short term corrosion section. Generally speaking, this area on all the long term samples appeared to have maintained the alumina film. Figure 66 shows a higher magnification of this area. The surface morphology in this zone has changed somewhat, but the basic passivated condition seems to persist. Moving slightly to the right on the sample, the mushroom-shaped corrosion product described in Figure 65 can be seen. In Figure 67, the SEM imaging is adjusted such that the growth is highlighted at the expense of the background surface detail. In doing so, it can be seen that the product growth previously mentioned in this section does not adhere closely to the surface at its source. Whenever a growth of this type appeared, it would be raised above the general surface around it. The process seemed to initiate with a crusty surface formation, followed by continued corrosion under a segment of that crust. The products beneath this segment continued to form, thereby lifting a portion of it, yielding a mushroom profile. A second type of corrosion was generally evident on the long term exposure group.

Figures 68, 69 and 70 show a succession of pictures of a nine-week sample, starting at the left edge and proceeding across its surface. The wave flow during formation on this sample went from left to right. Besides the obvious white scaly formations of the type just described, this sample shows pitting taking place. Close study showed that the areas of the wave fronts and vortices that contained melt

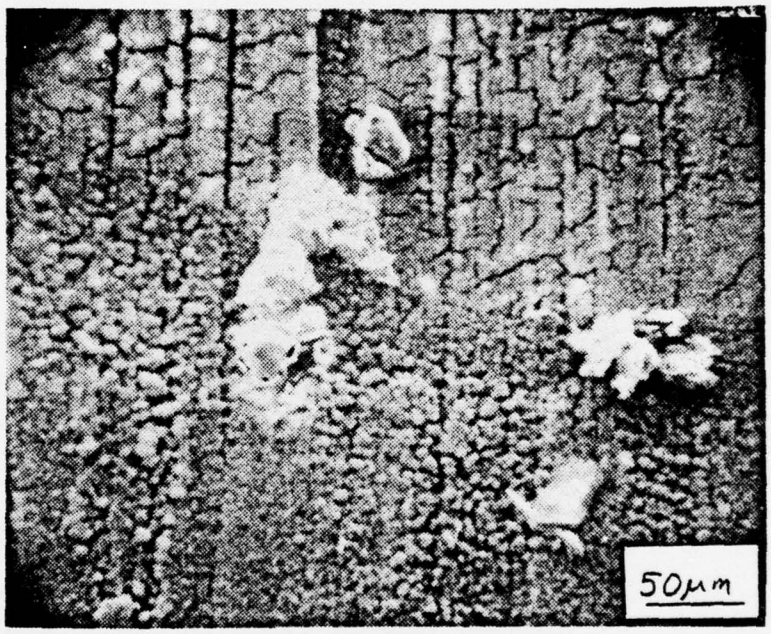

Figure 66. 280x SEM picture of bond zone passivation at trailing edge of wave of five-week exposure sample (Al over Steel).

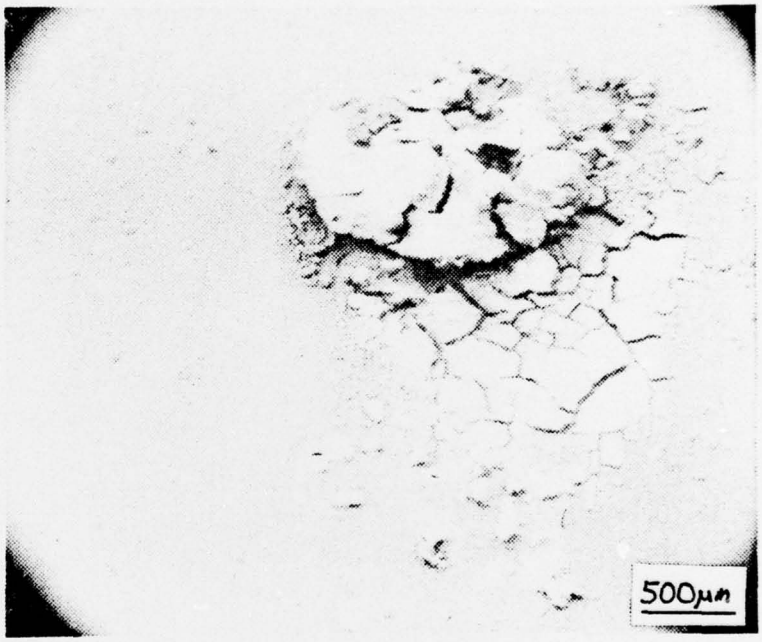

Figure 67. 27x SEM photograph of mushroom-shaped corrosion product on five-week exposure sample.

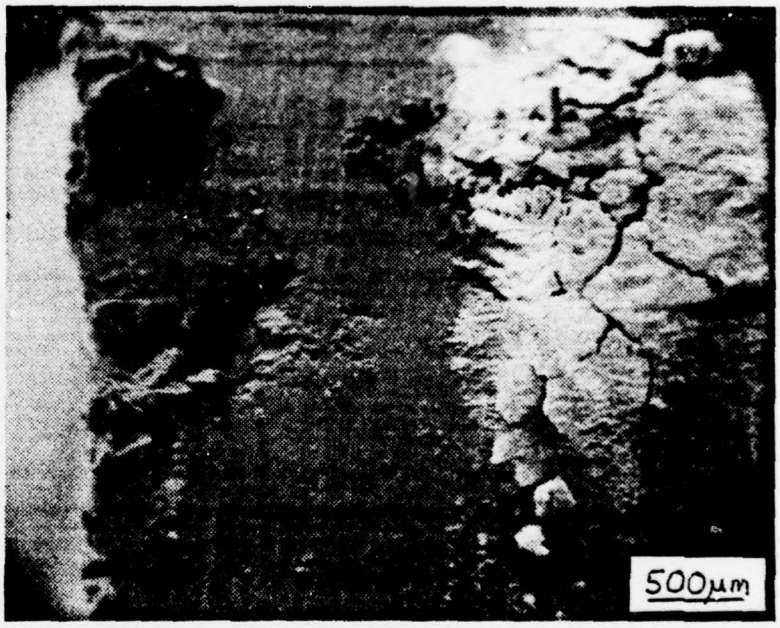

Figure 68. 27x SEM picture of nine-week exposure sample showing pitting and mushroom corrosion product build-up (Al over Steel).

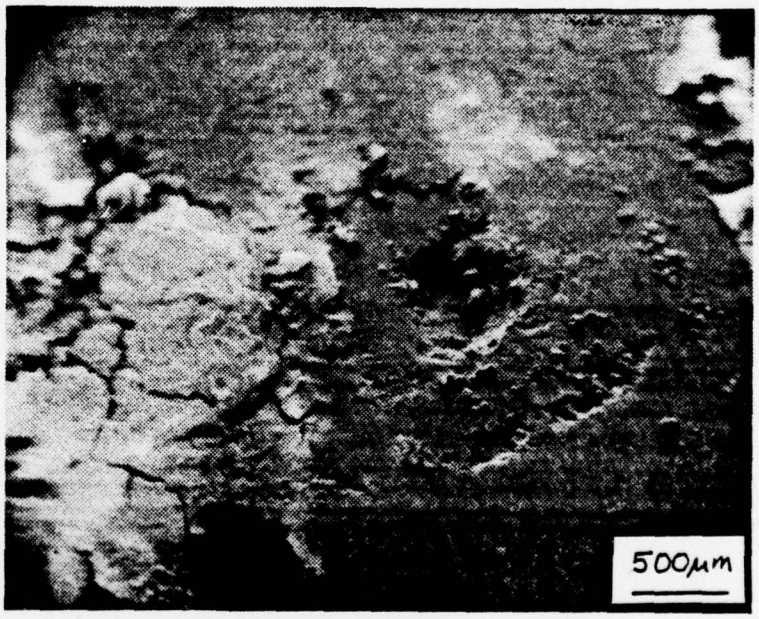

Figure 69. 27x SEM picture of nine-week exposure sample showing mushroom corrosion growth and melt pitting in wave (Al over Steel).

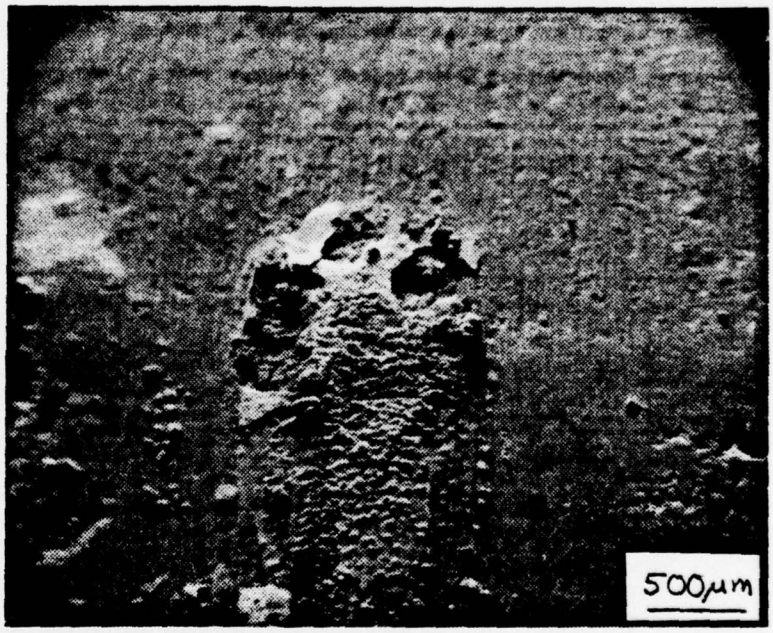

Figure 70. 27x SEM picture of nine-week exposure sample showing pitting, corrosion product growth, and wave outline (Al over Steel).

from the explosive formation were selectively corroded away on the long term specimens. This wasn't observed on the previous specimen because the vortex was devoid of melt. Penetration seemed to be quite deep but the bottoms of the pits were still clearly visible. Obviously no precipitation of a corrosion product of the melt took place at the pitting sites. This represented a second and quite different type of corrosion found in the long term exposure group.

IV. CONCLUSIONS

The following conclusions have been reached as a result of this study:

1. The explosively bonded triclad transition joint known as Detacouple® is susceptible to galvanic attack at the aluminum to steel interface when exposed to a periodic artificial sea water spray environment.

2. Accelerated anodic dissolution occurs in a narrow band on the 1100 aluminum at its interface with the steel.

3. Both aluminum and steel experience single metal electrochemical corrosion while in a periodic artificial sea water spray environment.

4. The aluminum ions in solution combine with OH^- ions to form hydrated alumina, $Al_2O_3 \cdot xH_2O$, or aluminum hydroxide, $Al(OH)_3$, and tend to precipitate out on the metal surfaces.

5. Gravitational flow of the electrolytic solution allows these compounds of aluminum to deposit on both the aluminum and the steel.

6. The hydrated alumina (aluminum hydroxide) tends to form a film on the aluminum and passivate it.

7. The anodic interface band tends to fill with the aluminum compounds and passivate.

8. Iron oxide, rust, forms on the steel in spite of the alumina film formation.

9. Not all areas of the bond zone are passivated. Continued corrosion occurs at certain, apparently more highly reactive, locations between wave crests. The exact source of this corrosion is unknown.

10. Melt formations within the steel wave vortex area and at the bond interface tend to be preferentially corroded.

V. RECOMMENDATIONS

The results of this study are of some assistance in understanding the passivating process of the hydrated alumina film on the Detacouple transition joint. Much further study is necessary though, to fully explain all of the corrosion processes that were observed. In particular, future investigations should focus on the following:

1. The mushroom-shaped corrosion buildup between wave crests appears to be very common. The extent and exact location of the material damage caused by this continued corrosion should be determined as a function of time and environment.

2. The melt material in the bond zone is corroded away in a sea water spray environment. The characteristics of the melt should be studied so that its formation during the bonding process could be minimized.

3. Mechanical testing should be performed on Detacouple® joints after they have been exposed to the sea water spray environment. This study would help determine the detrimental effects of the two types of continued corrosion cited.

4. A study to characterize the explosion-bond profile as a function of distance in from the surface should be undertaken. This study would be designed to determine the nominal penetration of such surface profile defects as melts and voids.

LIST OF REFERENCES

1. Alwitt, R. S., "The Growth of Hydrous Oxide Films on Aluminum," Journal of the Electrochemical Society, v. 121, p. 1322-1328, October 1974.

2. Banker, J. G. and C. R. McKenney, Explosion-Bonded Metals for Marine Structural Applications, paper presented to the Society of Naval Architects and Marine Engineers, San Diego section, San Diego, California, 18 November 1970.

3. Corrosion of Engineering Materials, short course presented at UCLA Extension, Los Angeles, 24-28 May 1976.

4. Defense Metals Information Center, Battelle Memorial Institute Memorandum 225, Explosive Bonding, by V. D. Linse, R. H. Wittman, and R. J. Carlson, p. 1-28.

5. Department of the Navy Military Specification MIL-J-24445 (SHIPS), Joint, Bimetallic Bonded, Aluminum to Steel, 1 March 1971.

6. E. I. duPont de Nemours & Company (Inc.), Specification EL-604M, Aluminum-Steel Transition Joints-Structural Applications, February 1971.

7. Fontana, M. G. and N. D. Greene, Corrosion Engineering, p. 30-33, McGraw-Hill, 1967.

8. Henthorne, M., "Cathode and Anodic Protection for Corrosion Control," Chemical Engineering, p. 73-79, 27 December 1971.

9. Henthorne, M., "Control the Process and Control the Corrosion," Chemical Engineering, p. 139-146, 18 October 1971.

10. Henthorne, M., "Corrosion Protection Via Coatings," Chemical Engineering, p. 103-108, 19 January 1972.

11. Henthorne, M., "Electrochemical Corrosion," Chemical Engineering, p. 102-106, 14 June 1971.

12. Henthorne, M., "Finding Answers to Corrosion Problems," Chemical Engineering, p. 97-102, 3 April 1972.

13. Henthorne, M., "Fundamentals of Corrosion," Chemical Engineering, p. 127-132, 17 May 1971.

14. Henthorne, M., "Good Engineering Design Minimizes Corrosion," Chemical Engineering, p. 163-166, 15 November 1971.

15. Henthorne, M., "Materials Selection for Corrosion Control," Chemical Engineering, p. 113-118, 6 March 1972.

16. Henthorne, M., "Measuring Corrosion in the Process Plant," Chemical Engineering, p. 89-94, 23 August 1971.

17. Henthorne, M., "Paints Prevent Corrosion," Chemical Engineering, p. 82-87, 7 February 1972.

18. Henthorne, M., "Polarization Data Yield Corrosion Rates," Chemical Engineering, p. 99-104, 26 July 1971.

19. Kester, D. R., I. W. Duedall, D. N. Conners and R. M. Pytokowicz, "Preparation of Artificial Seawater," Limnology and Oceanography, v. 12, p. 176-178, December 1967.

20. Naval Ship Research and Development Center Report 28-117, Aluminum Deckhouse Corrosion Control by W. Strasberg and O. C. Vreeland, 5 April 1972.

21. Naval Ship Research and Development Center Report 8-951, Results of 1- and 2-Year Corrosion Tests of Explosion-Bonded, Aluminum/Steel, Welding-Transition Joints, by R. B. Niederberger, 27 September 1971.

22. Pourbaix, M., Atlas D'Equilibres Electrochimiques, p. 168-172, Gauthier-Villars, 1963.

23. Scully, J. C., Fundamentals of Corrosion, p. 63-105, Pergamon Press, 1966.

24. Sienko, M. J. and R. A. Plane, Chemistry, p. 424-463, McGraw-Hill, 1961.

25. Tomashov, N. D., Theory of Corrosion and Protection of Metals, p. 367-393, MacMillan, 1966.

26. Trueb, L. F., "An Electron Microscope Investigation of Explosion-Bonded Metals," Transactions of the Metallurgical Society of AIME, v. 242, p. 1057-1065, June 1968.

27. Uhlig, H. H., Corrosion and Corrosion Control, p. 42-46, Wiley, 1971.

INITIAL DISTRIBUTION LIST

		No. Copies
1.	Defense Documentation Center Cameron Station Alexandria, Virginia 22314	2
2.	Library, Code 0142 Naval Postgraduate School Monterey, California 93940	2
3.	Department Chairman, Code 69 Department of Mechanical Engineering Naval Postgraduate School Monterey, California 93940	2
4.	Professor A. J. Perkins, Code 69Ps Department of Mechanical Engineering Naval Postgraduate School Monterey, California 93940	5
5.	Assistant Professor Terry McNelley, Code 69Mc Department of Mechanical Engineering Naval Postgraduate School Monterey, California 93940	1
6.	LT Michael R. Keelean USN Naval Reactors Representative Office Energy Research and Development Administration General Delivery Naval Base Branch Post Office Charleston, South Carolina 29408	4